Chemical Geology 574 (2021) 120155

Contents lists available at ScienceDirect

Chemical Geology

journal homepage: www.elsevier.com/locate/chemgeo

On the origin of saline compounds in acidic salt flats (Central Andean Altiplano)

JuanJosé Pueyo [a,*], Cecilia Demergasso [b,c], Lorena Escudero [b,c], Guillermo Chong [d], Paulina Cortéz-Rivera [d], Jorge Sanjurjo-Sánchez [e], Virginia Carmona [f], Santiago Giralt [g]

[a] Facultat de Ciències de la Terra, Universitat de Barcelona, c/Martí i Franquès, s/n, 08028 Barcelona, Spain
[b] Centro de Biotecnología, Universidad Católica del Norte, Antofagasta, Chile
[c] Centro de Investigación Científica y Tecnológica para la Minería, Antofagasta, Chile
[d] Departamento de Geología, Universidad Católica del Norte, Antofagasta, Chile
[e] Instituto Universitario de Xeoloxía, Universidade da Coruña, A Coruña, Spain
[f] Institut Joan Amigó, L'Espluga de Francolí, Spain
[g] Geosciences Barcelona (Geo3BCN-CSIC), Barcelona, Spain

ARTICLE INFO

Keywords:
Salar de Gorbea
Acidic brines
OSL dating
$\delta^{34}S_{VCDT}$
$\delta^{18}O_{VSMOW}$
$\delta^{2}H_{VSMOW}$
Sulfate recycling
Jarosite
Andean salt flats
Microbial sulfur oxidation
Thiotrophic microbial community

ABSTRACT

Volcanism, aridity, and endorheism converge in the central zone of the Andean Cordillera (Bolivia, Chile, and Argentina, between latitudes 19° S and 27° S). The Gorbea and Ignorado basins are pristine Andean sites in which the transfer of saline compounds from endogenous to exogenous environments occurs. In this area the regional volcanic rocks display strong argillic alteration, with Al and Fe (alunite, jarosite) and Ca (gypsum/anhydrite) sulfates. Native sulfur is also present in paleosolfataras. The Gorbea salt flat is covered by a discontinuous layer of selenitic gypsum of varying thickness (maximum 2 m). The discontinuity of the layer as well as its variable thickness is due to the fact that the original bed has been partially destroyed mainly by dissolution but also by deflation. Saline pond brines (Cl-SO_4-Na [-Mg]) are strongly acidic reaching pH values lower than 2. The high temperature processes that caused the hydrothermal alteration in the Gorbea and Ignorado basins occurred in the Miocene (14 Ma) coinciding with a wet period that reached 9 Ma. Subsequently, the weather up to 120 ka was predominantly hyper-arid with a less arid interval between 6 and 3 Ma and the epithermal sulfates were recycled in saline lakes mainly in the Late Pleistocene wet period (120 to 11.7 ka). Evolution into the current salt flat occurred in the mid-early Holocene (11.7 to 4 ka), through a salt lake that first evolved into a 'salina' environment that gave rise to a selenitic gypsum layer (6.4 ka), and later to the final dryness. The highest values of $\delta^{34}S_{VCDT}$ and $\delta^{18}O_{VSMOW}$ found in the selenitic gypsum layer (+20‰ and + 28‰, respectively) show that the recycling was locally produced, mainly from isotopically heavier hypogene sulfates. The $\delta^{18}O_{VSMOW}$ (and less clearly, $\delta^{34}S_{VCDT}$) values are higher in the basal part of the gypsum crust (about +27‰), which suggests an initial hypogene source that decreased towards the top due to mixing with supergene sulfate inputs. Bacterial activity, although catalyzing the supergene reactions, does not appear to have had a significant influence on the isotopic composition of sulfates. The crystallization water of the gypsum is isotopically lighter in the basal part of the selenitic layer ($\delta^{18}O_{VSMOW} \approx +7‰$), which indicates that the brines of the saline lake were still poorly evolved. These brines evolved to heavier (approximately +13‰) towards the top of the layer and towards the center of the salt flat, before the final drying. The partial destruction of the selenitic gypsum layer occurred during more recent wet periods over the last 4 ka that have been identified in wetlands and lakes in the Central Andean area. Isotopic data ($\delta^{34}S_{VCDT}$ and $\delta^{18}O_{VSMOW}$) clearly suggest that sulfates in the saline compounds and evaporites from the entire Central Andean arid area have mostly a thermal origin with contributions from atmospheric deposition and locally, near the Pacific coast, marine aerosols. In addition, the great difference in altitude (approximately 3000 m) between the Altiplano and the lands located to the west, up to the Pacific coast, generated a constant flow of groundwater containing saline compounds that gave rise, to the salt flats of the basins located in lower topographic areas (Atacama, Punta Negra, Hilaricos, Soledad, Tamarugal, Salar de Pintados, Salar Grande) throughout the Cenozoic. Such salt flats have lower $\delta^{34}S_{VCDT}$ and $\delta^{18}O_{VSMOW}$ values

* Corresponding author.
E-mail addresses: jjpueyo@ub.edu (J. Pueyo), cdemerga@ucn.cl (C. Demergasso), lescudero@ucn.cl (L. Escudero), gchong@ucn.cl (G. Chong), jorge.sanjurjo.sanchez@udc.es (J. Sanjurjo-Sánchez), vcarmona@tinet.cat (V. Carmona), sgiralt@ictja.csic.es, sgiralt@geo3bcn.csic.es (S. Giralt).

https://doi.org/10.1016/j.chemgeo.2021.120155
Received 27 March 2019; Received in revised form 23 July 2020; Accepted 2 March 2021
Available online 23 March 2021

mostly for two reasons: the secular mixing with atmospheric sulfate, and the isotope fractionation related to repetitive dissolution (or leaking)—migration—precipitation along the hydraulic gradient, a process that occurred throughout a large part of the Cenozoic. The last process also explains that the evaporites of some of these salt flats (e.g., Salar de Atacama, Salar Grande) display very high Cl/SO_4 ratios.

1. Introduction

Continental evaporites are commonly generated in intramountain lakes of arid lands by the precipitation of soluble compounds when the solubility product of involved minerals is exceeded. These soluble compounds, present in the watershed, are leached by the hydrological system towards the lowest parts where lakes are located. The origin of solutes is diverse: recycled old evaporites, sulfide oxidation products, thermal fluids and atmospheric deposition compounds, among others. Much of the continental evaporites, as often happens in Europe, are the result of recycling of old evaporites exhumed for geodynamic reasons (Utrilla et al., 1992; Taberner et al., 2000; Cendón et al., 2004). Recycling is also present in the Central-Andean area, where the Pleistocene paleo-salt flats are recycled into recent salt flats (Alonso, 1991; Alonso et al., 1991). The slow-rated accumulation of nitrate by atmospheric deposition is the main source in hyperarid desert areas where nitrogen compounds caused by biological activity strongly decrease. This was the case for nitrate deposits in the Atacama Desert (Böhlke et al., 1997; Reich and Bao, 2018) and, to a lesser extent in other arid areas such as the Mohave Desert, USA, Kumtag Desert, China, and the Transantarctic Mountains, Antarctica (Ericksen, 1981; Qin et al., 2012; Lybrand et al., 2016). In areas of intense volcanism, alteration of extensive rock volumes affected by thermalism and magmatic volatile compounds are the main source of solutes (Momenzadeh, 1990; Pueyo et al., 2001; Wörner et al., 2018). Evaporation of pore brines formed by mixing of basinal brines and leaking fluids from the altiplanic salt flats has been reported for the Central Andean area (Leybourne and Cameron, 2006; Leybourne et al., 2013; Rissmann et al., 2015). Meteoric and thermal waters transport the solutes up to lakes, whose hydrology depends on the local aridity. In addition, marine and volcanic aerosols and atmospheric deposition are other sources of solutes in hyperarid areas (Chong, 1994; Böhlke et al., 1997; Rech et al., 2003; Chong et al., 2020; Godfrey and Alvarez-Amado, 2020).

More than one hundred intramountain basins with salt lakes and salt flats (Stoertz and Ericksen, 1974; Chong, 1984) have been identified in the arid Central Andean Altiplano (Bolivia, Chile, and Argentina, between 19° and 27° S latitude). Of these basins only the Gorbea and Ignorado salt flats contain strongly acidic brines (pH between 2 and 4). The local acidity has been attributed to the release of sulfuric acid by oxidation of volcanic native sulfur and by pervasive hydrothermal alteration of the country rocks in their catchments (Cornejo, 1987), which are affected by high sulfidation epithermal systems (Sillitoe, 1999) that decreased their buffering capacity (Risacher et al., 2002). The alteration process has generally been defined as 'solfataric alteration' and also involves the formation of sulfuric acid and other acids generated by the reaction of meteoric water with magmatic gases. The effect of alteration on the rock-forming minerals in the volcanic rocks has been interpreted as acid hydrolysis (Sillitoe, 1993). Sulfuric gases oxidize when they reach the surface and commonly form solfataras with the precipitation of native sulfur.

Hydrothermal alteration related to Lower Miocene local volcanic activity has been studied in the Gorbea area (Cerro Bayo Complex; Cornejo, 1987). Other studies that recognize the importance of the involved fluids (Alpers and Brimhall, 1988; Deyell et al., 2005; Arancibia et al., 2006; Bissig and Riquelme, 2010) were carried out in the Precordillera at approximately the same latitude as the salt flats studied here. The Gorbea and Ignorado salt flat basins are unique environments where evaporites, including Al-Fe hydroxysulfates, are generated from magmatic-hydrothermal sources across a relatively small area (a few tens of kilometers) (Escudero et al., 2013; Karmanocky and Benison, 2016). Miocene volcanism generated acid gases that provided the anions (mostly chloride and sulfate), and the associated thermalism caused alteration of the country rocks, releasing cations (mainly sodium and magnesium). In the Gorbea and Ignorado basins, in addition to the low rock-buffering capacity, the oxidation of sulfur and iron of sulfides generated acidic brines that triggered the solubilization of other metals, mostly aluminum and iron (Risacher et al., 2002).

Numerous studies on the mineralogy, geochemistry and microbiology of acid drainage areas have been performed in places where iron-sulfide oxidation has occurred, including Tyrrell, Chandler, Gilmore, and Hann lakes in Australia (Long et al., 1992; Alpers et al., 1992; Macumber, 1992; Benison et al., 2007; Dickson and Giblin, 2009), wastes and weathered outcrops in sulfide mining areas in Chile (Dold and Fontboté, 2001; Dold and Fontboté, 2002; Dold and Spangenberg, 2005; Diaby et al., 2007; Spangenberg et al., 2007; Parra et al., 2011; Korehi et al., 2013; Smuda et al., 2014) eastern U.S.A. (Hammarstrom et al., 2005), southern Spain (Romero et al., 2006; Frost et al., 2007; Egal et al., 2008), and in coal mining areas in Nova Scotia, Canada (Zodrow et al., 1979). The Australian lakes and coal mining areas that display acidic waters have been compared here (even though they are not thermally affected areas) because they are useful analogues for mineralogical and microbiological studies.

Another primary source of acid drainage that has been studied is caused by the magmatic-related thermalism involved in epithermal deposits, as has been described at Mount Rainier (John et al., 2008) and other volcanic areas (Africano and Bernard, 2000; Varekamp et al., 2009). In addition to supergene environments, sulfuric acid can be produced throughout different stages of hydrothermal alteration, mainly by SO_2 disproportionation (Rye et al., 1989). The acidic mineral paragenesis found on the surface of Mars (Aubrey et al., 2006; Tosca and McLennan, 2006; Davila et al., 2008; Marion et al., 2009; Thollot et al., 2012), which is related to volcanism, makes terrestrial acid drainage areas of great interest as environmental analogues (Benison and Goldstein, 2002; Fernández-Remolar et al., 2005; Squyres and Knoll, 2005; Benison and Bowen, 2006; West et al., 2010; Benison, 2019). In addition, extremophile organisms living in these environments are of interest in the search for the environmental boundaries of life (Mormile et al., 2009; Benison and Karmanocky III, 2014; Escudero et al., 2018).

Although bacterial activity increases the rate of sulfo-oxidation reactions due to enzymatic catalysis (Newman and Banfield, 2002), the isotopic effects associated with the bacterial oxidation of reduced sulfur compounds are not yet well known (Fry et al., 1986; Hubbard et al., 2009; Pellerin et al., 2019). In this sense, oxidation experiments of reduced sulfur compounds in biotic and abiotic conditions carried out in the laboratory (Taylor et al., 1984; Balci et al., 2007, 2012, 2017; Brunner et al., 2008, 2012; Müller et al., 2013a, 2013b) were a major source of data on the isotopic behavior of sulfo-oxidation. In these experiments, the isotopic composition of oxygen in the sulfate produced by oxidation is basically conditioned by the isotopic exchange of sulfite and other intermediate sulfoxy species, with the water oxygen or with the dissolved oxygen (Betts and Voss, 1970; Müller et al., 2013a).

This paper aims to demonstrate the importance of the recycling of sulfur compounds between the internal geological cycle and the salt flats, as well as their timing in the context of the Andean paleoclimate. The study was conducted mainly around the Gorbea salt flat because, although similar to many others in the context of the Andean Altiplano, it has acidic brines. Due to the practical absence of other acidic salt flats in the Andean context we had to look for acidity analogues in other

places, even in different geodynamic contexts, as well as in leaching experiments related to sulfide mining. The isotopic study of sulfates in the altered country rocks in the salt flat, their evolution over time, and their comparison with data obtained from other places in the Atacama Desert, allow us to visualize a behavior model relevant to the Andean Range and other places with similar geodynamic settings.

1.1. Setting

The Gorbea and Ignorado salt flats are located within two adjacent intra-volcanic basins in the Andean Cordillera at approximately 4000 m. a.s.l. (meters above sea level) (Fig. 1a, b). The Gorbea salt flat (25° 24′ S, 68° 40′ W) has an approximate area of 30 km^2 and a catchment of approximately 320 km^2. The Ignorado salt flat (25° 30′ S, 68° 37′ W) is much smaller (0.7 km^2; catchment area of about 37 km^2; Risacher et al., 2002). The catchments of both salt flats consist of andesitic and dacitic stratovolcanoes (Lastarria, Plato de Sopa, Cerro Bayo) and are part of the Miocene-Holocene volcanic arc (de Silva, 1989; Scheuber et al., 1994; Richards and Villeneuve, 2002) that extends within the Central Andes between 16° and 28° S latitude. Stratovolcanoes in the volcanic arc coexist with rhyodacitic ignimbrite sheets with an age of approximately 20 Ma. The oldest Miocene volcanoes around the salt flats are collapsed and eroded, and they expose their hydrothermally altered cores, where tuffs are bleached and replaced by argillic associations, which greatly

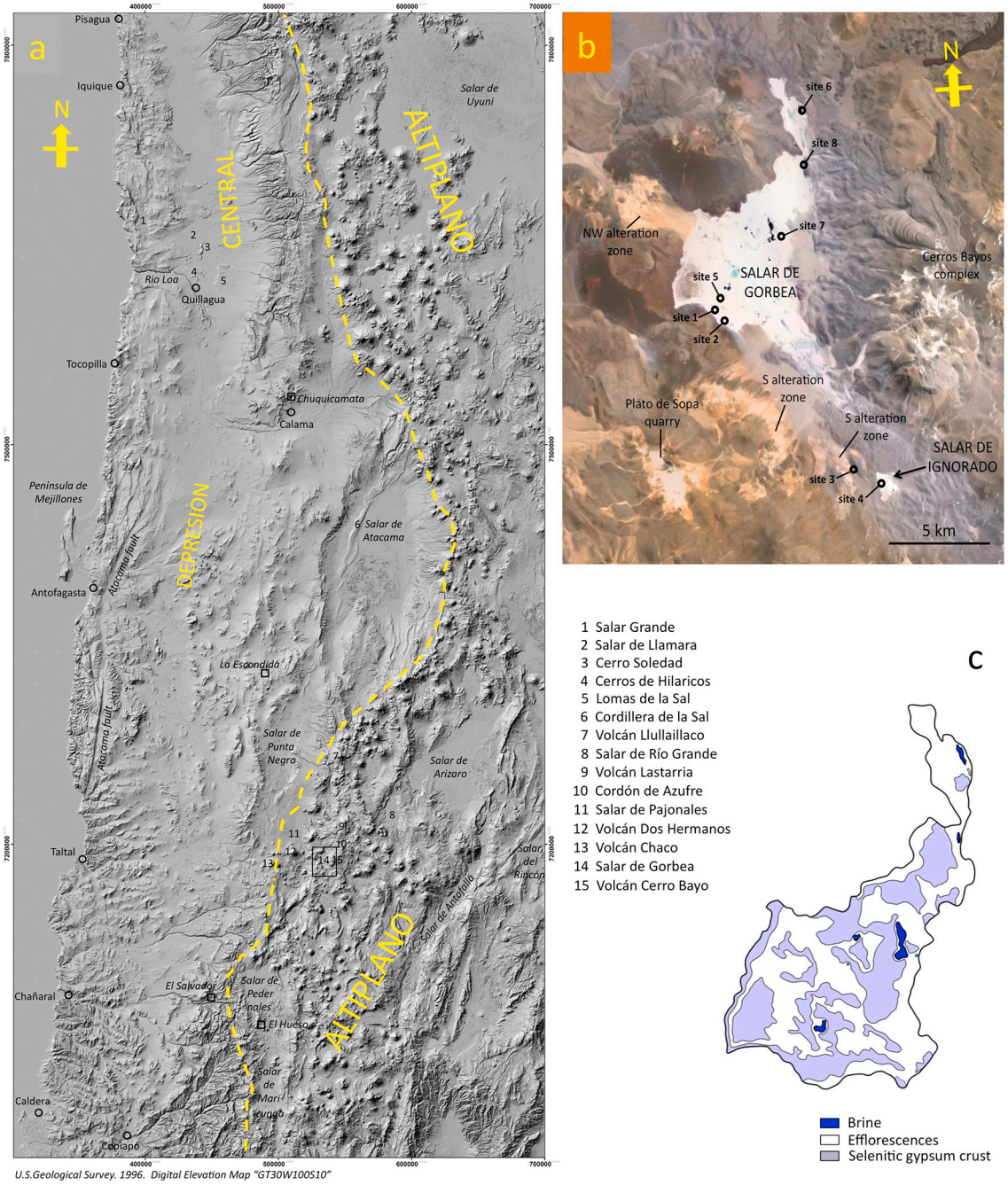

Fig. 1. **(a)** General view from the Pacific Coast to the Altiplano between 19°30′ to 27°30’ S latitude. Sites referred in the text are indicated on the map with numbers. **(b)** Map of the Gorbea salt flat and the surrounding area. The main sampling sites for water and solids and main volcanoes are indicated. The geographic coordinates of the 103 individual solid samples and 7 water samples are reported in Tables 1 and 2. **(c)** Distribution of the preserved gypsum crust on the Gorbea salt flat surface (Cortéz, 2014).

increase their permeability (Cornejo, 1987). The deeper altered parts contain hydrothermal breccias with extreme silicification, alunite and gypsum. The Upper Miocene stratovolcanoes are well preserved with solfataras in their upper parts (Cornejo, 1987). All of the solfataras in the catchment are inactive but there are still active solfataras in the vicinity (Lastarria volcano). The hypogene alunite has been K-Ar dated at Cerro Bayo (19.2 ± 3.9 Ma) and at other volcanoes nearby (Chaco and Dos Hermanos, from 18.1 to 21.1 Ma), although the latter is outside the salt flat catchment (Naranjo and Puig, 1984; Cornejo, 1987). Supergene alunite and jarosite mostly correspond to subsequent weathering processes associated with previous humid phases. There is no local information about the age of the supergene processes, but Ar-Ar dating at several sites to the east in the Andean Precordillera (El Salvador and Coya porphyries and El Hueso epithermal deposits at about 27° S latitude) indicate weathering ages of 15, 8, 4, and 0 Ma (Bissig and Riquelme, 2010).

The basement of the volcanic chain crops out to the east in the Precordillera and is mainly composed of Upper Paleozoic intrusive and volcanic rocks (Naranjo and Puig, 1984; Naranjo, 1986) with Ordovician-Devonian metasedimentary sequences (Ramirez and Gardeweg, 1982) and Triassic-Jurassic marine sedimentary rocks (carbonates, evaporites) and tephras. There is also evidence of continental Cenozoic sediments in the Altiplano, including evaporites related to the evolution of the Andean magmatic arc (Alonso, 1991).

The climate near the western margin of the Andean Altiplano is semiarid with some winter and summer precipitation (approximately 300 mm·yr^{-1} as rain or snow). The climatic evolution in this part of the Andean Ranges, based on lacustrine sequences, geomorphology, and archaeology studies, reveals nearly persistent aridity from the Middle Miocene to the present (Fig. 2; Alonso et al., 1985; Alonso and Viramonte, 1987). That persistent aridity favored the development of salt flats and the preservation of the original volcanic morphologies. The aridity was modulated over time with hyperarid phases, especially near the Pacific coast, and was only interrupted by a wetter phase in the late Pleistocene between 120 (or 70 depending on the latitude and elevation) and 11 ka BP. Large lakes developed in the Altiplano of Peru and Bolivia during this period and reached a maximum extent around 29 ka BP (Vita-Finzi, 1959; Hastenrath, 1971; Igarzábal, 1991) and affected almost all current southward salt flats. Therefore, many of the salt flats contain paleoshores and paleosalt bodies that are currently being recycled (Alonso et al., 1984; Alonso, 1991). Aridity returned in the Holocene driving the development of the recent salt flats. Finally, a wetter climatic pulse occurred between 3000 and 2500 years BP caused by the partial dissolution of the salt flat crusts (Igarzábal, 1979).

2. Methods

The chemical composition of brines and waters was analyzed using

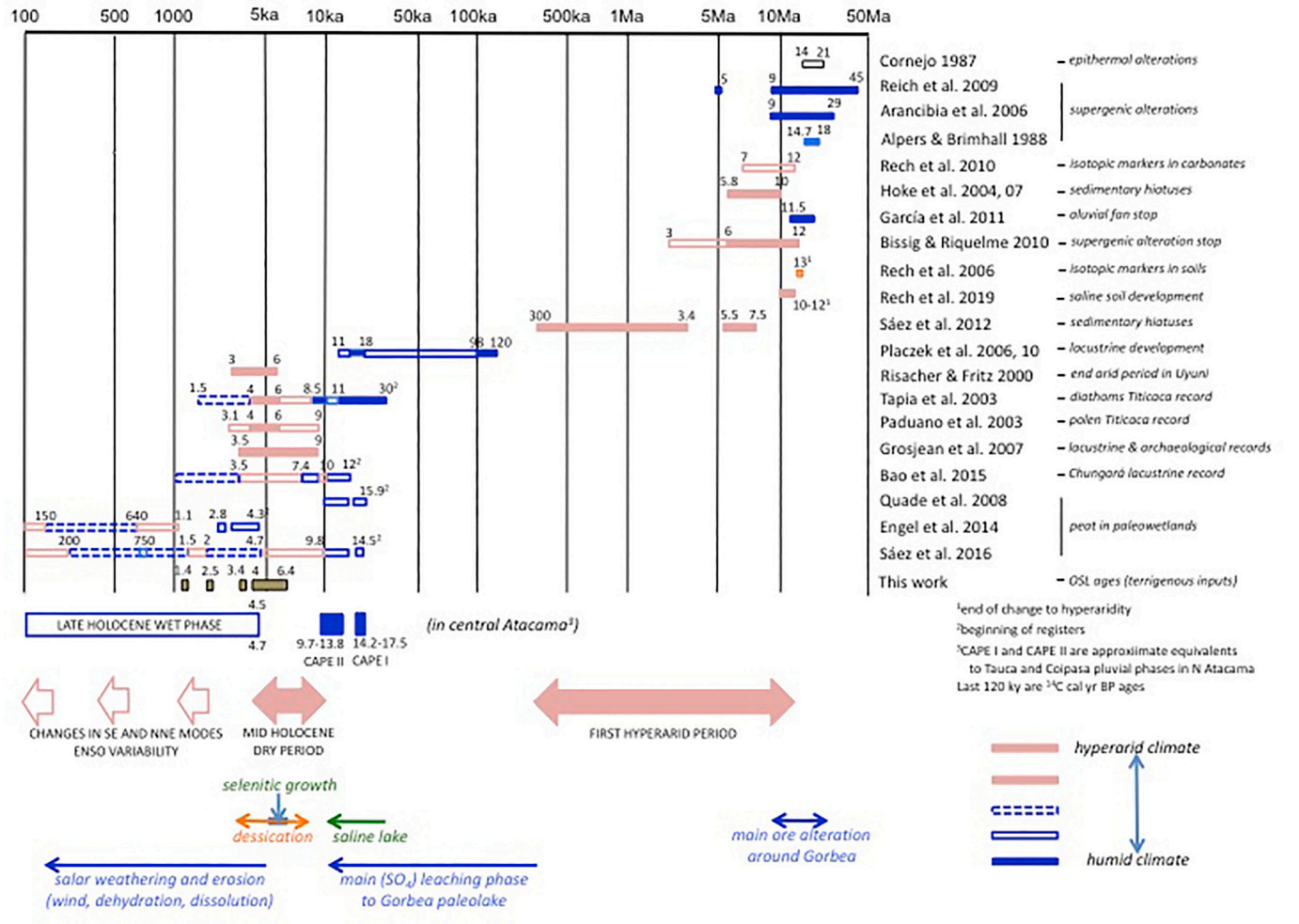

Fig. 2. Compilation of available data of the main aridity phases in the Atacama Desert (*s.l.*) since the Miocene. The timing of saline inputs and the Gorbea salt flat evolution are indicated in the lower part. '*This work*' data correspond to terrigenous inputs to the gypsum layer. The OSL data indicate that the gypsum layer developed from 6.4 to 4 ka BP. (Engel et al., 2014; García et al., 2011; Hoke et al., 2004; Hoke et al., 2007; Placzek et al., 2010; Quade et al., 2008; Reich et al., 2009; Sáez et al., 2012)

titration and ICP-OES (inductively coupled plasma – optical emission spectroscopy). Titration with $AgNO_3$ and an Ag specific electrode as endpoint detector was used to measure Cl^-. A Perkin-Elmer Optima 3200RL ICP spectrometer with cross-flow nebulizer was used to measure Na, K, Ca, Mg, Li, B, Si, S (for SO_4^{2-}), Fe, Mn, and Al. Calibration was made with 4 solutions prepared from commercial standard solutions (High Purity Standards, Charleston SC, U.S.A.) that are certified traceable to NIST materials. Samples were diluted in the range x20 to x200 depending on their concentration, and triplicate analyses were done for samples and standards. The isotopic composition of waters and brines (δ^2H_{VSMOW} and $\delta^{18}O_{VSMOW}$) was determined by IRMS (isotope-ratio mass spectrometry). To analyze δ^2H_{SMOW} the samples were treated in all cases by pyrolysis at 1350 °C. A 0.15 μL water aliquot was used and the H_2 produced was chromatographically purified and analyzed on a DELTA PLUS XP THERMOFISHER spectrometer with an accuracy of 1‰. To analyze $\delta^{18}O_{SMOW}$ in fresh water samples, 0.5 mL of water was equilibrated with a CO_2 (0.3%) - He mixture for 18 h in a GasBench connected online to a MAT-253 THERMOFISHER spectrometer with an accuracy of 0.2‰. Water samples with TDS higher than 2 wt% were treated by pyrolysis and the produced CO was analyzed in the same way as for δ^2H, with an accuracy of 0.4‰. Certified IAEA standards VSMOW2 ($\delta^2H = 0.0$; $\delta^{18}O = 0.0$), IAEA SLAP2 ($\delta^2H = -428.0$; $\delta^{18}O = -55.5$) and three secondary standards were used: LAB ($\delta^2H = -43.2$; $\delta^{18}O = -6.70$), MAR ($\delta^2H = -0.7$; $\delta^{18}O = -0.71$), NEU ($\delta^2H = -79.1$; $\delta^{18}O = -11.51$). The isotopic compositions of dissolved sulfate ($\delta^{34}S_{VCDT}$, $\delta^{18}O_{VSMOW}$) were determined from $BaSO_4$ precipitated by adding an excess of Ba^{2+} at pH 3 under boiling conditions. $\delta^{34}S_{VCDT}$ was determined in an online elemental analyzer-IRMS using standards NBS-127, IAEA-SO5, and IAEA-SO6 (and the local standard YCEM = +20.3‰) with an accuracy of ±0.4‰. $\delta^{18}O_{VSMOW}$ was determined with an online pyrolyzer-IRMS using the standard NBS-127 and the secondary standards H_2SO_4 = +13.2‰ and YCEM = +17.6‰ as references, with an accuracy of ±0.5‰ for duplicate analyses.

The mineralogy of both the solid samples from the salt flat surface and the rocks from the catchment was determined by XRD (X-ray diffraction) and semi-quantitatively estimated using RIR (reference intensity ratio) calculations (Tables 1 and 2). Extremely labile and deliquescent salts from the efflorescences were determined by transmission-XRD after confining samples between sheets of Mylar® (10 μm) film. The isotopic analyses ($\delta^{34}S_{VCDT}$, $\delta^{18}O_{VSMOW}$) were performed on sulfate minerals as described above for dissolved sulfate. Samples were previously dissolved in distilled water and the solution was filtered at 0.45 mm in order to separate the insoluble fraction. δ^2H_{VSMOW} and $\delta^{18}O_{VSMOW}$ values of the crystallization water were determined from selected pure gypsum, jarosite, and alunite samples using T-controlled pyrolysis (Rohrssen et al., 2008; Arbiol et al., 2014; slightly modified to change the thermal gradient). The position of the crucible inside the pyrolizer tube was modified in order to achieve a higher temperature than the dehydration of the minerals, without breaking down the sulfate group. The temperatures of OH loss, in the case of alunite and jarosite, and of crystallization water loss in the case of gypsum, were previously checked with a thermogravimeter, and a T-pyrolysis of 600 °C was chosen for all three minerals. The quantitative efficiency of the extraction was proved in all samples by the wt% H and wt% O parameters provided by the spectrometer itself by comparing them with a sulfanilamide standard (O = 18.58 wt%; H = 4.68 wt%). Coumarin ($\delta^2H = +82.3$), biphenyl ($\delta^2H = -41.0$) (Schimmelmann, 2014) and IAEA-CH7 ($\delta^2H = -100.3$), with an accuracy of ±5‰, were the standards used for δ^2H_{VSMOW} analyses because they are solid with a suitable thermal behavior in the pyrolyzer. The standards for $\delta^{18}O_{VSMOW}$ were IAEA-602 and IAEA-603, with an accuracy of ±0.6‰. All of the solid samples were studied with ESEM-EDS (environmental scanning electron microscopy – energy dispersive spectrometry). Hard rock chips and unconsolidated sediment were observed without treatment in the low vacuum mode (approximately 0.5 mbar of water) to obtain backscattered electron images and EDS X-ray spectra.

2.1. OSL dating

The sampling was performed at night using a pick to excavate up to 30 cm of the weathered surface, between 1 and 1.2 m above the base of the gypsum layer. The samples were transported in opaque black plastic bags to prevent alteration by exposure to light. All of the subsequent processing was performed in a dark chamber that was only illuminated during the analysis with red light. The process consisted in dissolving gypsum with water in a rotary drum agitator to release clastic sediment trapped during crystal growth. The nature and concentration of the clastic particles were estimated by XRD, which confirmed that the main minerals were quartz and plagioclase. Due to the scarcity of the clastic fraction, 400 g of selenitic gypsum was dissolved and, given the low solubility of gypsum (2 $g \cdot L^{-1}$), approximately 200 L of water was necessary in a manipulation that lasted for 5 months.

The clastic sediment was sieved to obtain the 63–300 μm size fraction. Minerals other than quartz were gravity removed using a centrifuge, and the remaining quartz etched with concentrated HF. Small quartz aliquots (~ 50 grains) were mounted on stainless steel disks and checked with infrared stimulation to ensure there was no contamination by other minerals. The quartz OSL signals were measured in an automated Risø DA-15 TL/OSL reader system equipped with blue (470 ± 30 nm) LEDs (light-emitting diodes) for stimulation and a coupled 9235QA PMT (photomultiplier tube). An optical 6-mm-thick Hoya U-340 filter was used (340 ± 80 nm emission) to measure the OSL signals. Laboratory doses were given using a $^{90}Sr/^{90}Y$ beta source mounted on the reader giving a dose rate of 0.110 ± 0.003 Gy s^{-1}. The SAR (single-aliquot regenerative) dose protocol (Murray and Wintle, 2000, 2003) was used to estimate the equivalent dose. The aliquots were preheated to 200 °C for 10 s (temperature chosen after performing a preheat test) and stimulated for 40 s at 125 °C before the OSL, and the test-dose response was measured after heating to 160 °C (TL at 5 °C s^{-1}). Both the first 0.8 s and the last 4 s of the OSL decay curves were integrated for signal measurement and background subtraction, respectively. Dose recovery tests were performed after the bleaching procedure and irradiation with beta doses similar to the calculated EDs (Murray and Wintle, 2003). The natural dose rate was estimated by measuring the K content with XRFS (X-ray fluorescence spectrometry), and the U and Th contents were assessed by ICP-MS. Conversion factors (Guerin et al., 2011) were used to assess the dose rate; the alpha contribution was neglected, and the beta-dose rate was corrected due to the removal of the etched layer from the quartz grains (Brennan, 2003). The water content and saturation of the bulk sample was assessed in situ, and the cosmic dose rates were calculated and corrected (Prescott and Hutton, 1994).

3. Results

3.1. The catchment of the salt flats

The drainage basins of the Gorbea and Ignorado salt flats contain volcanic edifices (Plato de Sopa to the SW of the Gorbea salt flat, Mayor to the NW, Cerro Bayo to the E; Cortéz, 2014) that underwent extensive hydrothermal alteration of the argillic, advanced argillic, and extreme silicification types (Cornejo, 1987). The mineral content of samples collected from outcrops in the W and S parts of the Gorbea basin (Table 1, Figs. 1 and 3a) reveal a mineral association containing opal CT, alunite, jarosite, hematite, kaolinite, gypsum, among other minor minerals such as birnessite. The country rock is cut by a fracture network that contains silica, alunite, and jarosite (Fig. 3b, c). The altered rock can be described as a silica sponge (mainly opal CT) whose pores are filled with alunite, gypsum, and less commonly, jarosite (Fig. 3d, e, f). Other more soluble sulfates and chlorides are present in minor proportions. Native sulfur deposits that formed in the paleosolfataras on top of the Plato de Sopa and Lastarria volcanoes contain extensive silica mixed with sulfur and fractures filled with fibrous gypsum and alunite. In addition to these minerals, a recent generation of jarosite was found near

Table 1
Geographic coordinates and main mineralogy of 73 solid samples corresponding to altered rocks and native sulfur of the salt flat catchment.

Sample reference	Field description	Latitude	Longitude	Plagioclase	K-feldspar	Pyroxene	Quartz	Opal CT	Kaolinite	Hematite	Goethite	Jarosite	Hydronium jarosite	Alunite	Natroalunite	Minamiitee	Gypsum	Hexahydrite	Starkeyite	Thenardite	Loeweite	Bloedite	Halite
Outer sediments and altered rocks in the catchment																							
1	Eolic gypsarenite, SE Gorbea	S-25º26'50.4"	W-68º38'51.3"				t										M						
7	P-2, slightly altered rock near salar margin, white patina	S-25º25'57.0"	W-68º41'08.6"	M													m		m				M
9	P-2 altered rock in the salar margin, salts inside cavities	S-25º25'57.0"	W-68º41'08.6"	M	M	m											m						
1e	SW 1a, white patina in altered rock	S-25º28'45.7"	W-68º39'47.1"						M	t							m						
2e	SW 1b, red patina in altered rock	S-25º28'45.7"	W-68º39'47.1"							M	m						t						
3e	SW 2a, white dust, gypsum filling fracture	S-25º28'45.7"	W-68º39'47.1"														M						
4e	SW 2b, gypsum in fissure + clayey altered material, ocher coloured	S-25º28'45.7"	W-68º39'47.1"											t			M						
5e	SW 3 silica with altered rock?, white yellowish	S-25º28'45.7"	W-68º39'47.1"					m							m		M						
6e	SW 4 silica (opal?)	S-25º28'45.7"	W-68º39'47.1"				M	m															
7e	SW 5 [similar to SW 3] silica with altered rock?, white yellowish	S-25º28'45.7"	W-68º39'47.1"					m						M	M		M						
8e	SW 6a [similar to SW 1b] red altered rock	S-25º28'45.7"	W-68º39'47.1"							m				m	M		m						
9e	SW 6b [similar to SW 1a] white patina	S-25º28'45.7"	W-68º39'47.1"														M						
10e	SW 7 [similar to SW3 and SW5] silica with altered rock?	S-25º28'45.7"	W-68º39'47.1"					m	M					m			m						
11e	SW 8a [similar to SW1b and SW6a] red altered rock	S-25º28'45.7"	W-68º39'47.1"					m		M							m						
12e	SW 8b cement between clasts, white	S-25º28'45.7"	W-68º39'47.1"												m		M						
13e	NW 1 altered part, white	S-25º23'31.8"	W-68º42'41.1"					m	m						M		t						
14e	NW 2 vacuoles filled rock ('honeycomb' like), white	S-25º23'31.8"	W-68º42'41.1"														M						
15e	NW 3 [similar to NW1] inner part of NW4, white	S-25º23'31.8"	W-68º42'41.1"					M	m						M		m						
16e	NW 4 outer part of NW3 (2 cm), ocher	S-25º23'31.8"	W-68º42'41.1"					M	m	m					M		m						
17e	NW 5 altered material, WHITE	S-25º23'31.8"	W-68º42'41.1"				m	M						m	M		m						
18e	NW 6 [similar to NW1 and NW3] inner part of NW7, white	S-25º23'31.8"	W-68º42'41.1"	m			m	M						M	M		m						
19e	NW7 outer part of NW6, eolic dust?, light brown	S-25º23'31.8"	W-68º42'41.1"				m	M		m				M	m		m						
20e	NW 8 [similar to NW5] alteration patina, white	S-25º23'31.8"	W-68º42'41.1"					M		t				M	m		m						
21e	S 1a filling in open fracture, greenish brown	S-25º29'11.4"	W-68º38'17.5"									M											
22e	S 1b under the patina, white	S-25º29'11.4"	W-68º38'17.5"					t						M		t							
23e	S 1c filling in fracture, yellow dust mixed with white material	S-25º29'11.4"	W-68º38'17.5"									m		M									
24e	S 1d rock with aplitic aspect?, pinkish	S-25º29'11.4"	W-68º38'17.5"					M						M			m						
25e	S 2a white patina	S-25º29'11.4"	W-68º38'17.5"							M				m	M	t							
26e	S 2b innermost part of the altered rock	S-25º29'11.4"	W-68º38'17.5"					M		M				M									
27e	S 3 alterd rock	S-25º29'11.4"	W-68º38'17.5"									m	m	M									
28e	S 4 altered rock with kaolinite? and gypsum	S-25º29'11.4"	W-68º38'17.5"					t		t				M			m						
29e	S 5a outer patina, yellow-white	S-25º29'11.4"	W-68º38'17.5"															M		m	m		M
30e	S 5b inner part of the altered rock, pinkish-white	S-25º29'11.4"	W-68º38'17.5"					M						M									
31e	S 6a [similar to 5a] in patina and filling cracks	S-25º29'11.4"	W-68º38'17.5"														m	M		m	m		M
32e	S 6b outer patina, red	S-25º29'11.4"	W-68º38'17.5"				M	M		M				t									
33e	S 6c altered bulk rock	S-25º29'11.4"	W-68º38'17.5"				M	m		M				M									
34e	S 7a compact dust mass, ocher	S-25º29'11.4"	W-68º38'17.5"									M	M										
35e	S7b yellow green crystals filling crack, ocher color as dust	S-25º29'11.4"	W-68º38'17.5"									M		m									
36e	S 8a almost loose surface material, white	S-25º29'11.4"	W-68º38'17.5"														m	m		M	M	M	m
37e	S 8b inner part of altered rock	S-25º29'11.4"	W-68º38'17.5"					M						M									
38e	S 9 altered rock (kaolinized?)	S-25º29'11.4"	W-68º38'17.5"					M						M									
39e	S 10a [similar to S5a, S6a and S8a] white material in surface and cracks	S-25º29'11.4"	W-68º38'17.5"											m				m			m		M
40e	S 10b altered rock (white material)	S-25º29'11.4"	W-68º38'17.5"					M		m				M									
PS-1	1, colored host material, dark red, Plato de Sopa volcano quarry	S-25º28'52.7"	W-68º43'13.1"				m			M													
PS- 1R	Host rock, Plato de Sopa volcano quarry	S-25º28'52.7"	W-68º43'13.1"				M	M															
PS-2	Native sulphur, Plato de Sopa volcano quarry	S-25º28'52.7"	W-68º43'13.1"			M																	
PS-3	2, colored material, Plato de Sopa volcano quarry	S-25º28'52.7"	W-68º43'13.1"				m	M						m			m						
PS-4	3, colored material, Plato de Sopa volcano quarry	S-25º28'52.7"	W-68º43'13.1"				t	m		t					M								
PS-5	Native sulphur with silica? Plato de Sopa volcano quarry	S-25º28'52.7"	W-68º43'13.1"			M	m																
PS-6	Silica? Plato de Sopa volcano quarry	S-25º28'52.7"	W-68º43'13.1"				M																
PS-7	Fibrous gypsum in cracks. Plato de Sopa volcano quarry	S-25º28'52.7"	W-68º43'13.1"														M						
GO-10 inf	Jarosite? + sediment. NE salar margin	S-25º22'35.0"	W-68º38'36.7"														M						
GO-10 med	Jarosite? + sediment. NE salar margin	S-25º22'35.0"	W-68º38'36.7"	m			m										M						
GO-10 sup	Jarosite? + sediment. NE salar margin	S-25º22'35.0"	W-68º38'36.7"														M						
GO-10 sup2	Jarosite + sediment. NE salar margin	S-25º22'35.0"	W-68º38'36.7"									m					m						M
GO-11	incrustations. NE salar margin	S-25º22'35.0"	W-68º38'36.7"														M	m	m				M
GO-12	Efflorescences/splash?. E salar margin	S-25º22'57.7"	W-68º38'25.9"																				M
GO-13-1	Jarosite? under regolith. E salar margin	S-25º23'49.3"	W-68º39'16.1"	m			m										M						
GO-13-2	Jarosite? under regolith. E salar margin	S-25º23'49.3"	W-68º39'16.1"				m										M						
GO-15	S. Fibrous gypsum filling centimetre-thick crack	S-25º29'11.4"	W-68º38'17.5"														M						
GO-16-1	S. Ferruginous fracture filling in reddish altered rock	S-25º29'11.4"	W-68º38'17.5"					M	m	M				t									
GO-16-2	S. Ferruginous fracture filling in whitish altered rock	S-25º29'11.4"	W-68º38'17.5"					M	M					m									
GO-17	Thin efflorescence. Small salt flat eastwards from Gorbea	S-25º25'56.3"	W-68º43'33.1"														t	m					M
GO-18	Terrigenous sediment, alteration of andesite	S-25º25'44.0"	W-68º42'22.4"	M	m		m										M						
GO-19	NW, alunite-sílica?	S-25º23'27.1"	W-68º42'50.5"					m						t	M		1						
GO-20	NW, alunite-sílica?	S-25º23'27.1"	W-68º42'50.5"					m	m						M		m						
GO-21	NW, alunite-sílica-hematite?	S-25º23'27.1"	W-68º42'50.5"					m						n		M	m						
GO-22-1	NW, alunite-hematite-sulphide?	S-25º23'22.8"	W-68º42'59.0"							M	m				M								
GO-22-2	NW, alunite-hematite-sulphide?	S-25º23'22.8"	W-68º42'59.0"							M	M			n	M								
GO-23	NW, alunite-hematite-jarosite?	S-25º23'22.8"	W-68º42'59.0"					m				M	M		m								
GO-24	NW, alunite-hematite-jarosite?	S-25º23'22.8"	W-68º42'59.0"										M	M									
GO-25	Recent jarosite coating of regolith. W saltflat edge, near road	S-25º26'04.6"	W-68º42'59.0"	m								M					m						
GO-26	SW, silica-alunite?	S-25º28'27.2"	W-68º39'54.9"				M																

SW, S, and NW in the field description indicate the main alteration areas sampled around the Gorbea salt flat. In the mineralogical descriptions, M = major, m = minor, and t = trace indicate the sample compositions.

the environment of the salt flat. This jarosite, 1 to 6 μm in size, was still wet and occurred as cement between clastic sediments around the salt flat (Fig. 1 Site 2). Recent jarosite was also found in minor amounts beneath the gypsum layer on the NE margin of the Gorbea salt flat (Fig. 1 Site 8).

The $\delta^{34}S_{VCDT}$ and $\delta^{18}O_{VSMOW}$ values of the sulfate in solid samples (Table 3, Fig. 4) and the $\delta^{18}O_{VSMOW}$ and $\delta^{2}H_{VSMOW}$ values of the crystallization water, which is present as H_2O in gypsum and as OH in the aluminum sulfates (Table 3, Fig. 5), were used as provenance markers. The lowest $\delta^{34}S_{VCDT}$ values (approximately −4‰) correspond to native sulfur for the Plato de Sopa volcano and to the southern and southwestern alterations around the Gorbea salt flat. Intermediate values are found in the northwestern alteration, whereas the highest values (up to +20‰) are present in the selenitic gypsum layer that spans most of the salt flat surface. The $\delta^{18}O_{VSMOW}$ values in sulfate also increase from the fibrous gypsum veins in native sulfur (+7‰) to the highest values in alunite samples in the epithermal alteration and in the selenitic gypsum from the salt flat (up to +28‰). The highest $\delta^{2}H_{VSMOW}$ values in the crystallization water are in selenitic gypsum (between −10 and − 50‰), while sulfate minerals from the alteration areas around the Gorbea salt flat have values between −25 and − 85‰ for alunite and from −60 to −110‰ for jarosite. The $\delta^{18}O_{VSMOW}$ values of the crystallization water are widely distributed between +5.5 and + 13‰ for selenitic gypsum, and are similar to those of the jarosite samples. The alunite values are more restricted (+7 to +10‰). Fibrous gypsum from veins in native sulfur has the lowest $\delta^{18}O_{VSMOW}$ value (+1.5‰) of all of the solid samples in the catchment and a $\delta^{2}H_{VSMOW}$ value of −79‰.

3.2. The brines in the Gorbea salt flat ponds

Extensive studies of the hydrochemistry in the area of the Gorbea and Ignorado salt flats have been previously reported (Risacher et al., 1999, 2002, 2003; Chong et al., 2015). The Gorbea watershed is characterized by a supply of water from the melting of snow and from aquifers (Risacher et al., 2002). The only place with permanent surface water input is located on the southern margin of the salt flat, although minor tributaries are evident on both the eastern (Cerro Bayo) and western margins; the latter is of only minor relevance. The brines in the salt flat are of the Cl - SO_4 - Na (− Mg) type and contain high concentrations of aluminum and boron (up to 2000 and 1000 $mg \cdot L^{-1}$, respectively) and lower concentrations of manganese, lithium, iron, and arsenic (Table 4; Escudero et al., 2013). Magnesium has higher concentrations than sodium only in the more evolved brines of the central ponds. In these ponds, as well as in those located in front of the fans in the eastern margin, the pH reaches values close to 1.

The isotopic composition of water from the tributaries of the Gorbea salt flat ($\delta^{2}H_{VSMOV}$ = −51.6‰ and $\delta^{18}O_{VSMOV}$ = −4.63‰; in sample Bofedal 3, Table 4) is representative of the free non-stagnant water in this part of the Altiplano. The main water entrances to the Gorbea salt flat are from the south, where there is a permanent surface current—and where the 'Bofedal 3' water sample was taken. There are also minor inputs from the east margin. In both cases, hydrological feeding is caused by the melt water from Cerro Bayo snow, a fact evidenced by the presence of small delta fans in the south and, with less development, on the eastern margin (Fig. 1b). The brines in the salt flat ponds show higher isotopic compositions, reaching positive values for oxygen. The isotopically heaviest brines are located in the west-central part of the salt flat surface (up to $\delta^{2}H_{VSMOV}$ -12.3‰ and $\delta^{18}O_{VSMOV}$ + 1.63‰; samples Gorbea 1, 2, and 5, Table 4). The isotopic compositions of dissolved sulfate in the more diluted waters and brines are for $\delta^{34}S_{VCDT}$ between +6 and + 8‰, and for $\delta^{18}O_{VSMOW}$ between +12 and + 15‰. In the more concentrated brines dissolved sulfate values reach close to $\delta^{34}S_{VCDT}$ + 9‰ and $\delta^{18}O_{VSMOW}$ + 15‰.

3.3. Gypsum and other salts in the Gorbea salt flat

The surface sediments of the salt flats are mostly composed of a partially eroded layer of primary selenitic gypsum. This layer is preserved in situ on a large part of the salt flat surface (Fig. 1c). The rest of the surface is presently covered by a several centimeter-thick cumulate of fallen selenitic crystals. A similar arrangement has been observed at the nearby salt flats Ignorado and Pajonales (about 10 km southeast and 30 km northwest, respectively). A non-eroded 3.5-m-thick vestige of the selenitic gypsum layer, as well as the contact between said layer and the substrate, is preserved on the NE margin of the Gorbea salt flat (Site 8 in Figs. 1b; 6c, d). The layer is composed of vertical gypsum crystals arranged in decimeter-thick strata. The efflorescent salts in the depressions around the ponds are mostly white, but in some central areas and in front of the alluvial fans on the eastern margin of the Gorbea salt flat, they display an intense yellow (Table 1, Fig. 6a) around the most acidic ponds (pH 2.6; Table 4). These efflorescences consist of a fine mixture of halite, magnesium sulfate (mainly hexahydrite), carnallite, minor amounts of aluminum and magnesium chloride-sulfates (kainite, magnesioaubertite), hydronium kainite, and very small amounts of jarosite (Fig. 6b). The yellow efflorescences have a sour taste and they darken wrapping paper because they contain non-neutralized sulfuric acid.

The selenitic gypsum series in the northeastern outcrop (Fig. 6c, d) is composed of two cycles. The lower cycle has relatively uniform values of $\delta^{34}S_{VCDT}$ (approximately +19‰) and $\delta^{18}O_{VSMOW}$ (+25 to +29‰). The upper cycle is more variable with $\delta^{34}S_{VCDT}$ between +15 and + 20‰ and lower values of $\delta^{18}O_{VSMOW}$ (+20 to +24‰; Table 3) than the lower cycle. Selenitic gypsum from the center of the salt flat shows relatively constant values ($\delta^{34}S_{VCDT}$ of approximately +12‰ and $\delta^{18}O_{VSMOW}$ of approximately +21‰; Fig. 4). The selenitic gypsum from the eastern part of the Ignorado salt flat has lower values ($\delta^{34}S_{VCDT}$ + 6‰ and $\delta^{18}O_{VSMOW}$ + 16‰), which are similar to the sulfate samples from the southwestern and southern alteration areas. The crystallization water also reflects significant isotopic changes in selenitic gypsum between the upper and lower cycles of the series (Table 3, Fig. 5). The lower cycle has relatively constant values for $\delta^{18}O_{VSMOW}$ (approximately +7 ± 1‰) and for $\delta^{2}H_{VSMOW}$ (−30 ± 10‰). The upper cycle has a trend with a lower slope (approximately +7) than the LMWL (local meteoric water line; between +8.1 and + 7.9; Chaffaut et al., 1998; Herrera et al., 2006) with an increase in the values towards the top of the sequence that is similar to the gypsum values from the central part of the salt flat (+12 to +13‰ for $\delta^{18}O_{VSMOW}$ and − 20 to −10 for $\delta^{2}H_{VSMOW}$). The $\delta^{34}S_{VCDT}$ and $\delta^{18}O_{VSMOW}$ values for the efflorescences (+10‰ and + 17‰, respectively) are slightly higher than those of the brines in nearby ponds.

OSL analyses allowed dating the gypsum crust. Contents of 0.20 ± 0.1 ppm, 9.05 ± 0.45 ppm and 0.14 ± 0.003% were assessed for U, Th, and K, respectively. Considering the obtained beta (0.31 ± 0.02 $Gy \cdot ka^{-1}$), gamma (0.48 ± 0.02 $Gy \cdot ka^{-1}$), and cosmic rates (0.41 ± 0.04 $Gy \cdot ka^{-1}$), this results in a dose rate of 1.20 ± 0.05 $Gy \cdot ka^{-1}$. OSL analyses of small aliquots provided 17 accepted aliquots (considering the requirements of SAR) from a total of 31 measured aliquots (Table 5). The obtained D_es ranged from 1.61 ± 0.30 Gy to 18.90 ± 7.91 Gy (Table 5), that can be joined in four groups of ages: 1.39 ± 0.10 ka (3 aliquots), 2.53 ± 0.24 ka (3 aliquots), 3.43 ± 0.42 ka (3 aliquots) and 6.37 ± 0.67 ka (11 aliquots). They can be interpreted as terrigenous inputs during wetter periods of the Late Holocene wet phase.

3.4. Data from saline compounds in the Atacama Desert and other altiplanic sources

In addition to considering previously published data (Böhlke et al., 1997; Carmona et al., 2000; Pueyo et al., 2001; Carmona, 2002; Rech et al., 2003; Bao et al., 2004; Leybourne et al., 2013), a series of samples located from west of the Altiplano, in the arid lands of the Salar de Atacama Basin and in the Chilean Central Depression, which are parts of

Table 2
Geographic coordinates and main mineralogy of 30 solid samples corresponding to evaporites and saline materials from the salt flat surface, mostly from the gypsum crust and efflorescences around ponds.

Sample reference	Field description	Latitude	Longitude	Plagioclase	Quartz	Jarosite	Alunite	Gypsum	Hexahydrite	Starkeyite	Thenardite	Loeweite	Bloedite	Kainite	K-Alum	Epsomite	Magnesioaubertite	Halite	Carnallite
Inner sediments of the salt flat																			
2	In situ' preserved selenitic gypsum, margin NE Gorbea salar	S-25°22′36.8"	W-68°38′38.2"					M										t	
3	Selenitic gypsum near site 5 (SE)	S-25°21′19.4"	W-68°38′24.6"					M											
4	Selenitic gypsum, site 5 W Ignorado salar	S-25°29′58.2"	W-68°37′28.5"					M											
5	Yellowish sediment under selenitic gypsum (near sample 2)	S-25°25′40.2"	W-68°41′17.9"		t	M		M										m	
6	Terrigenous sediment under efflorescence in site 5	S-25°21′19.4"	W-68°38′24.6"	M	m			m										m	
8	P-1, red regolith at the edge of water: white incrustation	S-25°25′43.1"	W-68°41′25.3"	m			t	M											
10	P-1, red regolith at the edge of water: red patina	S-25°25′43.1"	W-68°41′25.3"	M		m	t	m											
11	Gypsum 1	S-25°25′40.2"	W-68°41′17.9"					M											
12	Efflorescence outside the brine, foto P-2 (dry)	S-25°25′57.0"	W-68°41′08.6"					m			M		m					t	
13	White efflorescence P-6 (dry)	S-25°24′10.7"	W-68°39′22.0"						M				m		m		t	M	m
14	Yellowish efflorescence P-1	S-25°25′43.1"	W-68°41′25.3"						M			t					m	M	m
15	Yellowish efflorescence near P-1	S-25°25′43.1"	W-68°41′25.3"						M								m	M	m
16	Yellow efflorescence P-6	S-25°24′10.7"	W-68°39′22.0"						M					m			m	M	m
17	White efflorescence P-1	S-25°25′43.1"	W-68°41′25.3"						M							M		M	
18	Recent white efflorescence P-5	S-25°25′25.2"	W-68°41′13.8"						M									M	
19	White efflorescence P-5	S-25°25′25.2"	W-68°41′13.8"						M	m								M	
20	Yellowish efflorescence P-1	S-25°25′43.1"	W-68°41′25.3"						M						t		m	M	m
GO-8	Yellow efflorescence, *E*-NE margin of salt flat	S-25°23′18.2"	W-68°38′39.3"						M	m				m			m	M	m
GO-14	Yellow efflorescence, E margin of salt flat	S-25°24′10.7"	W-68°39′22.0"						M	m				m			m	M	m
GO-9-1	Selenitic gypsum, outer NE margin of salt flat	S-25°22′35.0"	W-68°38′36.7"					M											
GO-9-2	Selenitic gypsum, outer NE margin of salt flat	S-25°22′35.0"	W-68°38′36.7"					M											
GO-9-3	Selenitic gypsum, outer NE margin of salt flat	S-25°22′35.0"	W-68°38′36.7"					M											
GO-9-4	Selenitic gypsum, outer NE margin of salt flat	S-25°22′35.0"	W-68°38′36.7"					M											
GO-9-5	Gypsite? between selenites, outer NE margin of salt flat	S-25°22′35.0"	W-68°38′36.7"					m										M	
GO-9-6	Microselenitic gypsum, outer NE margin of salt flat	S-25°22′35.0"	W-68°38′36.7"					M											
GO-9-7	Slightly altered selenitic gypsum, outer NE margin of salt flat	S-25°22′35.0"	W-68°38′36.7"					M										t	
GO-9-8	Slightly altered selenitic gypsum, outer NE margin of salt flat	S-25°22′35.0"	W-68°38′36.7"					M										t	

(*continued on next page*)

Table 2 (*continued*)

Sample reference	Field description	Latitude	Longitude	Plagioclase	Quartz	Jarosite	Alunite	Gypsum	Hexahydrite	Starkeyite	Thenardite	Loeweite	Bloedite	Kainite	K-Alum	Epsomite	Magnesioaubertite	Halite	Carnallite
Inner sediments of the salt flat																			
GO-9-9	Slightly altered selenitic gypsum, outer NE margin of salt flat	S-25°22′35.0″	W-68°38′36.7″					M										t	
GO-9-10	Slightly altered selenitic gypsum, outer NE margin of salt flat	S-25°22′35.0″	W-68°38′36.7″					M										t	
GO-9-11	Gypsite? between selenites, outer NE margin of salt flat	S-25°22′35.0″	W-68°38′36.7″					M										t	

In the mineralogical descriptions, M = major, m = minor, and t = trace indicate the estimated relative mineral amounts.

the Atacama Desert (*s.l.*) were analyzed here (Tables 6 and 8 in Appendix). The samples from the Salar de Atacama Basin were taken from cores from boreholes drilled by lithium extraction companies and from outcrops of the Cordillera de la Sal. The samples from the Chilean Central Depression were from outcrops located in the Llamara - Hilaricos, Salar Grande, and Lomas de la Sal areas. In general terms, the isotopic compositions of sulfur, and mainly oxygen, are in the Gorbea environment ($\delta^{34}S_{VCDT}$ + 7.5‰ and $\delta^{18}O_{VSMOW}$ + 20.7‰ average values in the watershed; $\delta^{34}S_{VCDT}$ + 16.3‰ and $\delta^{18}O_{VSMOW}$ + 22.7‰ average values in the salt flat surface; Table 3, Fig. 4), higher than those commonly found in the Atacama Desert ($\delta^{34}S_{VCDT}$ + 6.0‰ and $\delta^{18}O_{VSMOW}$ + 12.8‰; Tables 6 and 8 in Appendix).

4. Discussion

4.1. Sulfate and pH behavior

Magnesium is the dominant cation in the most evolved brines after the efflorescent precipitation of sodium phases (halite, thenardite) on the salt flat surface. The sulfate concentration only exceeds chloride on the eastern margin of the salt flat due to the groundwater inputs from Cerro Bayo. The less concentrated water of a stream that feeds the Gorbea salt flat at its southern end (Fig. 1, Site 3; sample 'Bofedal 3', Table 4) and which represents the most dilute surface water found in the area (17 $g \cdot L^{-1}$) has pH 6. In the rest of the sampled surface waters and brines the pH is lower, reaching the lowest values in the central ponds, where acidity increases with evapoconcentration (Benison and Bowen, 2015; Escudero et al., 2018) due to hydrolysis caused by Fe^{3+} and Al^{3+} (McArthur et al., 1991; Ayora et al., 2013). In addition, pH also decreases on the central-eastern shore of the salt flat, where the low pH is clearly related to inputs coming from the old solfataras located at the top of Cerro Bayo. The Cerro Bayo Complex, which is the highest mountain in the area, collects a significant amount of snow during the winter. The snow melts slowly and carries the sulfur oxidation products (a mixture of HSO_4^- and SO_4^{2-} depending on the pH; threshold at pH 1.99) through streams and underground aquifers to the salt flat margin. Aeolian recycling of efflorescences may be the cause of subsidiary pH fluctuations (Benison and Bowen, 2015). The high concentrations of aluminum and other metals (iron, manganese) in the waters and brines are related to the low pH, which is below the solubility threshold of Fe oxyhydroxides. Boron, lithium, and, to a lesser degree, arsenic also show significant concentrations, which is common in the Altiplano salt lakes due to the strong hydrothermal inputs. The arsenic concentration (up to 25 $mg \cdot L^{-1}$ in the evolved brines of the Gorbea salt flat) and speciation are controlled by the Eh, pH, and iron species present in the waters (Demergasso et al., 2014).

The local acidity has been attributed to the overlap of two factors (Risacher et al., 2002): i) the significant occurrences of volcanic native sulfur around the salt flat catchments (Naranjo, 1986; Froger et al., 2007), with the release of sulfuric acid by biotic and abiotic oxidation, and ii) the strong hydrothermal alteration of the country rocks, which practically overrides their buffering capacity (Long and Lyons, 1992; Benison and Bowen, 2013). Of both factors, probably the most important is the anomalous accumulation of volcanic native sulfur in the area, mainly revealed in the Lastarria volcano (Aguilera et al., 2016) and in the so-called Cordon de Azufre (Naranjo, 1985, 1988). Lastarria volcano is located northwards, outside the hydrological basin of the Salar de Gorbea, but the volcanoes Cerro Bayo and Plato de Sopa, both with important paleosolfataras, and forming part of the Cordon de Azufre, delimit the Gorbea salt flat watershed. A similar setting occurs almost symmetrically on the Argentinian side, where exploitable amounts of thenardite precipitated in the Rio Grande salt flat due to the presence of the 'Mina Julia' paleosolfataras (Lurgo Mayón, 1999). However, a greater contribution of OH^- from the alteration of silicate minerals, mostly feldspar hydrolysis, has buffered the pH of the brines. In the Gorbea, Ignorado, Pajonales and Río Grande basins, common alteration

products such as Ca^{2+} and Na^{+} are combined with a strong local contribution of solfataric SO_4^{2+}, which are added to those produced by sulfur oxidation, being the locally predominant cause of sulfates (gypsum or thenardite) in the flat salt crusts.

The oxidation of iron sulfides is the main source of acidity in mineralized areas and this is increased in the Gorbea salt flat by ferrolysis and catalyzed by sulfur (and iron) oxidizing bacterial activity (Benison and Bowen, 2015; Quatrini et al., 2017; Escudero et al., 2013) combined with the scarce buffer capacity of the bedrock (Risacher et al., 2002). Given the structure of the communities observed in brines and sediments of the Gorbea salt flat, a considerable fraction of the chemolithoheterotrophic and facultative chemolithoautotrophic microorganisms oxidize reduced sulfur compounds thereby conserving energy for fixing carbon dioxide. The predominant phyla are *Proteobacteria*, *Firmicutes*, and *Actinobacteria* (Escudero et al., 2018). The microbial communities in this acidic and salty lake have differential features compared with known Acid Mine Drainage (AMD) ecosystems (Bond et al., 2000a, 2000b; Tyson et al., 2004; García-Moyano et al., 2012; González-Toril et al., 2003, 2015) and with other salt lakes in the Andean region (Demergasso et al., 2004, 2008; Mandakovic et al., 2018): i) the absence of iron oxidizing microorganisms that are abundant in AMD systems is explained by those systems being supported by the oxidation of sulfide minerals with high iron content instead of by the oxidation of elemental sulfur; ii) the abundance of chemolithoheterotrophic and facultative chemolithoautotrophic instead of chemolithoautotrophic microorganisms found in AMD ecosystems, and iii), the absence of known halotolerant and/or halophilic heterotrophic taxa that commonly inhabit salt lakes and salterns, including those at acidic pH levels in Australia (Escudero et al., 2018; Johnson et al., 2015; Zaikova et al., 2018), suggests that oligotrophy is important for survival in this acidic and salty extreme ecosystem; iv) the absence of proton consuming metabolisms like the sulfate-reducers, also common in salt lakes and salterns (Escudero et al., 2018). The sulfur oxidation pathways mostly represented in Gorbea are SOX (thiosulfate-oxidizing multienzyme system) and the dissimilatory sulfite reductase dsrAB, which operates in the reversed direction (oxDsrAB) (Escudero et al., 2018). Some of the described inhabitants have not been reported before in extreme natural acidic environments.

Sulfur-oxidizing bacteria can oxidize reduced sulfur compounds (sulfides, native sulfur) using the dissolved oxygen in water or oxygen from the water molecule itself (Lloyd, 1967, 1968; Toran and Harris, 1989). Because the solubility of gaseous oxygen in water strongly decreases with the concentration of brines (Geng and Duan, 2010), the use of oxygen from the water itself to oxidize reduced sulfur compounds is strongly predominant. It is known that, at low temperature conditions there is no isotopic exchange between the oxygen of sulfate and the oxygen of water (Lloyd, 1968; Chiba and Sakai, 1985), and that all the exchange occurs between intermediate oxidation species (mainly sulfite SO_3^{2-}) and water (Table 7; Müller et al., 2013a, 2013b). In the case of SOX and oxDsrAB pathways all the oxygen atoms required to produce sulfate came from the dissociation of water (Gosh and Dam, 2009; Brunner et al., 2012), a fact that leads to a major contribution of the oxygen isotope composition of water to the oxygen isotope composition of the produced sulfate (Brabec et al., 2012; Brunner et al., 2012). Oxygen isotopic enrichments between sulfate and water during sulfide oxidation in oxic-anoxic and biotic-abiotic conditions have been reported from laboratory experiments at pH 7 (Brabec et al., 2012) and from sulfide lixiviation experiments at pH $\leq$ 3 (Balci et al., 2012) (Table 7). Values of $\varepsilon^{18}O_{SO4\text{-}H2O} = +8 \pm 0.4‰$ were obtained (Balci et al., 2012) at similar pH conditions than in the Gorbea environment, although the isotopic enrichment attributable to bacterial activity is scarce (Balci et al., 2007). In the case of sulfur there are no significant isotopic enrichments during sulfide oxidation (Brunner et al., 2008; Balci et al., 2007, 2012) except in some cases due to kinetic effects (Alam et al., 2013; Balci et al., 2017) (Table 7). Experimentally measured isotopic enrichments (Table 7) are compatible with the data obtained in the Gorbea environments (Table 3, Fig. 4). Oxygen in sulfate undergoes a significant enrichment with respect to the oxygen of the water and with respect to the oxygen dissolved in the water, while the sulfur remains unaffected during supergene alteration. The only changes in the $\delta^{34}S_{VCDT}$ of the resulting sulfate minerals are those related to precipitation that also affects the $\delta^{18}O_{SO4}$ (Thode and Monster, 1965). However, the enrichments observed in Gorbea have not allowed us to discriminate isotopic effects specifically attributable to bacterial activity. Also, the previously reported results of experiments on biotic and abiotic sulfide oxidation show an increase in reaction rate by enzymatic catalysis by up to six orders of magnitude (Singer and Stumm, 1970; Newman and Banfield, 2002), yet do not show significant isotopic differences between biotic and abiotic processes.

4.2. Sulfate provenance

$\delta^{18}O_{VSMOW}$ values between +21 and + 28‰ with $\delta^{34}S_{VCDT}$ values higher than +15‰ in the 11 analyzed samples of Gorbea alunites (Table 3, Fig. 4) reflect high temperature oxidation processes related to hypogene high-sulfidation thermal alteration (Hedenquist et al., 1993; Simmons et al., 2005). Intermediate $\delta^{34}S_{VCDT}$ values of alunite between +8 to +15‰ are commonly interpreted as due to the effect of late (and partial) replacements by lower temperature steam-heated or magmatic-steam fluids in solfataric stages (Deyell et al., 2005). $\delta^{34}S_{VCDT}$ values of alunite lower than +8‰ (and down to 0‰) are attributed to solfataric and supergene stages (Rye et al., 1989, 1992; Seal II et al., 2000). Jarosite and gypsum have lower $\delta^{34}S_{VCDT}$ and $\delta^{18}O_{VSMOW}$ values than the coexisting alunite in Gorbea, showing a trend with a slope of approximately +0.8 (Fig. 4). Lower values and similar trends (between +0.5 and + 0.3) have been reported for other epithermal fields (Creede, Colorado USA) with magmatic-hydrothermal alunite and supergene jarosite (Rye, 2005). The lowest values of $\delta^{34}S_{VCDT}$ (−3 to +3‰) are found in gypsum veins from native sulfur of the Plato de Sopa volcano and in sulfates from the southern alterations around the salt flat, and they reflect the original values of magmatic sulfur close to 0‰ (Coleman, 1977). The oxidative weathering of reduced sulfur compounds occurs without isotopic fractionation of sulfur (Seal II, 2006), since it is a generalized process that does not distinguish the different isotopic masses. Given the low $\delta^{34}S_{VCDT}$ of native sulfur in the area (Table 3, Fig. 4), sulfates that are formed in this way virtually inherit the isotopic composition of native sulfur only affected by the fractionation linked with gypsum precipitation ($\varepsilon^{34}S_{gyps\text{-}dissSO4} = +1.65‰$; Thode and Monster, 1965). The oxidation can only have been produced in the presence of meteoric water (mainly snow) without other contributions, since it has occurred at around 5000 m of altitude. Also, low values of $\delta^{34}S_{VCDT}$ in the S and SW alteration areas (Table 3, Fig. 4) are related to S^0 oxidation inputs coming from the nearby Cerro Bayo and Plato de Sopa paleosolfataras ($\delta^{34}S_{VCDT} = -1.5‰$ for Plato de Sopa native sulfur). The lowest $\delta^{18}O_{VSMOW}$ values are also found in the gypsum veins from the Plato de Sopa sulfur quarry, which were caused by sulfur oxidation in the presence of isotopically light water from snow (about $\delta^{18}O_{VSMOW}$ -50‰; $\delta^{2}H_{VSMOW}$ -120‰; Aravena et al., 1999, Ohlanders et al., 2013; Fig. 8). The jarosite samples around Gorbea mostly correspond either to veins (Fig. 3b and c) in the volcanic country rocks generated in the solfataric stage (with alunite as described in Rye et al., 1989), or to recent supergene cements in terrigenous sediments around the salt flat margins (Fig. 6e and f).

The $\delta^{2}H_{VSMOW}$ and $\delta^{18}O_{VSMOW}$ values of hypogene alunite reflect the presence of brines and changes in temperature conditions. The evolution of magmatic-hydrothermal systems is a source of brines produced by exsolution that display $\delta^{2}H_{VSMOW}$ and $\delta^{18}O_{VSMOW}$ values of approximately −40 and + 5‰, respectively (Bethke et al., 2005). When the brines leave the magma chamber, they alter the volcanic country rock to form alunite-silica bodies in areas of intense leaching (Bethke et al., 2005). Alunite and jarosite from epithermal alterations around the Gorbea salt flat show (except for the sample from the Plato de Sopa

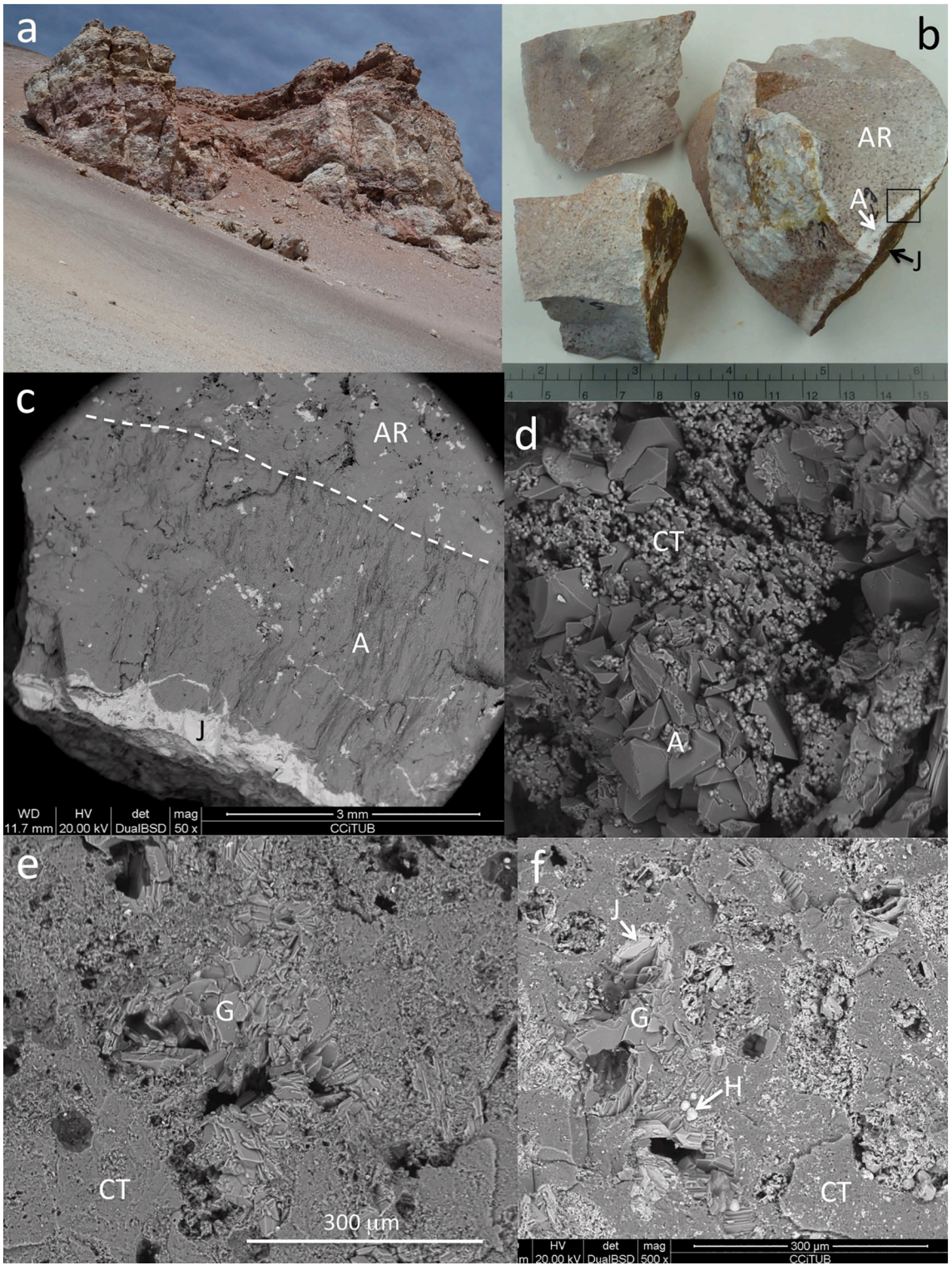

Fig. 3. Petrography of altered rocks cropping out in the catchment. **a)** Altered tephra outcrop in the southern part of the Gorbea Basin. Images b and c correspond to the southern area. **b)** Rock fragments formed by silica and alunite with minor amounts of gypsum. The fragment on the right shows two orthogonal veins bearing alunite (white-A) and jarosite (dark green-J). **c)** Detail of one of the veins (square in b): altered rock (AR) formed by silica and alunite (gray) with minor amounts of gypsum (dark) and jarosite (white), fibrous filling of the alunite vein (A) and central filling of jarosite (J). SEM back-scattered electron microscopy image. **d)** Euhedral alunite (A) in porous microcrystalline silica (CT opal). SW alteration area. SEM image. **e)** Opal and euhedral gypsum (G). SEM image. **f)** Opal, euhedral gypsum, euhedral jarosite (J), and minor amounts of hematite (H); e) and f) correspond to the NW alteration area. SEM back-scattered electron microscopy image. (For interpretation of the references to color in this figure legend, the reader is referred to the web version of this article.)

Table 3
Isotopic data from solid samples grouped according to the salt flats and catchment areas.

Sample ref.	*Composition (type)*	*In SO_4*		*In composition water*	
		$\delta^{18}O_{VSMOW}$	$\delta^{34}S_{VCDT}$	$\delta^{18}O_{VSWOW}$	$\delta^{2}H_{VSMOW}$
Inner sediments in the salt flats					
2	selenitic gypsum, site8	+24.4	+19.4		
GO-9-1	selenitic gypsum, site8, upper part series1	+21.9	+20.2	+12.3	−14.5
GO-9-2	selenitic gypsum, site8	+21.9	+18.8	+12.6	−18.0
GO-9-3	selenitic gypsum, site8	+23.6	+17.4	+7.9	−48.9
GO-9-4	selenitic gypsum, site8	+23.3	+18.6	+7.5	−53.2
GO-9-5	selenitic gypsum, site8	+20.,7	+15.4	+5.5	−33.2
GO-9-6	selenitic gypsum, site8	+22.7	+19.1		
GO-9-7	selenitic gypsum, site8	+28.5	+19.1	+7.2	−36.3
GO-9-8	selenitic gypsum, site8	+27.2	+19.4	+6.0	−27.0
GO-9-9	selenitic gypsum, site8	+26.5	+19.2	+6.5	−18.5
GO-9-10	selenitic gypsum, site8	+25.8	+19.3	+6.3	−28.2
GO-9-11	selenitic gypsum, site8, lower part series1	+25.8	+19.4	+8.2	−44.0
3	Selenitic gypsum, salar centre, site 5	20.5	+12.0	+12.8	−10.9
11	Selenitic gypsum, salar centre, site 1	+22.0	+13.6		
4	Selenitic gypsum W margin (Salar de Ignorado)	+16.4	+6.3	+10.8	−23.5
12	Efflorescences around Gorbea ponds	+17.0	+10.3		
16	Efflorescences around Gorbea ponds	+18.1	+10.1		
GO-8	Efflorescences around Gorbea ponds	+18.3	+10.3	+7.0	−25.8
GO-14	Efflorescences around Gorbea ponds	+18.5	+10.2	+10.8	−40.4
Outer sediments and altered rocks in the catchment					
1	Eolic gypsarenite	+20.8	+10.8		
GO-13-1	Gypsum in regolith (outer E margin)	+25.2	+13.9		
GO-13-2	Gypsum in regolith (outer E margin)	+22.6	+13.7		
GO-11	Gypsum (with halite incrustations NE margin)	+23.7	+14.9	+12.3	−43.0
14e	Gypsum filling vacuoles (NW margin)	+17.4	+8.0		
GO-15	Gypsum in alterations (S, SW areas)	+18.8	+3.7	+9.1	−50.3
3e	Gypsum in alterations (S, SW areas)	+17.2	+0.4	+8.8	−45.9
9e	Gypsum in alterations (S, SW areas)	+20.8	+11.0		
5e	Gpsum + Na-alunite (SW area)	+14.8	+3.1		
12e	Gpsum + Na-alunite (SW area)	+12.3	−2.6		
13e	Alunite (NW area)	+27.9	+9.9	+7.8	−36.8
17e	Alunite (NW area)	+25.7	+17.2	+9.1	−29.9
GO-19	Alunite (NW area)	+28.5	+15.0		
GO-20	Alunite (NW area)	+23.8	+12.4		
GO-21	Alunite (NW area)	+23.2	+16.8		
GO-22-1	Alunite (NW area)	+20.4	+12.7	+8.1	−76.4
GO-22-2	Alunite (NW area)	+25.4	+7.8	+8.9	−85.7
22e	Alunite (S area)	+24.7	+0.5	+9.7	−26.2
24e	Alunite (S area)	+27.6	+2.8		
28e	Alunite (S area)	+13.4	+8.1		
38e	Alunite (S area)	+26.0	+1.9	+9.4	−29.5
21e	Jarosite (S area)	+20.2	−2.2	+10.6	−107.2
35e	Jarosite (S area)	+21.2	−2.7	+12.9	−97.5
GO-23	Jarosite (NW area)	+15.0	+3.9	+10.1	−63.0
GO-24	Jarosite (NW area)	+15.9	+6.5	+7.0	−64.8
GO-25	Jarosite (recent in W margin, road)	+20.6	+12.8	+13.1	−78.6
5	Jarosite (recent? near sample 2 under selenites)	+27.9	+19.5		
sps1	Native sulfur (Plato de Sopa volcano)		−5.6		
sps2	Native sulfur (Plato de Sopa volcano)		−5.4		
PS-2	Native sulfur (Plato de Sopa volcano)		−1.7		
PS-5	Native sulfur (Plato de Sopa volcano)		−4.1		
PS-4	Alunite bed into native sulfur	+11.7	0.0	+8,9	−59.6
PS-7	Fibrous gypsum into native sulfur	+8.0	−2.9	+1,5	−78.5

The samples from the surfaces of the salt flats consist of selenitic gypsum and efflorescences, and the samples from the catchment include gypsum, alunite, jarosite, and native sulfur. All of the samples are grouped by composition as in Figs. 4 and 5. The data correspond to the isotopic compositions of sulfur and oxygen in the sulfate and of hydrogen and oxygen in the crystallization water.

volcano quarry) an isotopic dispersion of the $\delta^{2}H_{VSMOW}$ and $\delta^{18}O_{VSMOW}$ values in crystallization water of 80‰ and 5‰, respectively. However, while the values for oxygen are similar, this does not happen in the case of hydrogen due to the large difference in the isotopic fractionation coefficient for both minerals (Rye and Alpers, 1997). The jarosite that is currently forming on the margins of the Gorbea salt flat shows $\delta^{34}S_{VCDT} = +12‰$ and $\delta^{18}O_{VSMOW} = +20‰$ in the sulfate and $\delta^{2}H_{VSMOW} = -80‰$ and $\delta^{18}O_{VSMOW} = +13‰$ in the crystallization water. In supergene and low temperature environments, there is little water-mineral isotopic fractionation of alunite and jarosite in OH (i.e., $\alpha^{2}H_{water\text{-}OH\ 25^{\circ}} = 1.004$ and is much lower for oxygen; Bird et al., 1989; Seal II et al., 2000). Thus, the values of $\delta^{2}H_{VSMOW}$ and $\delta^{18}O_{VSMOW}$ reflect the isotopic compositions of the water in which the jarosite precipitated, and indicate that it has been strongly affected by evaporation. These values are similar to those measured in the southern alteration area of Gorbea that correspond to its late (supergene) origin. Recent cements and displacive growths of alunite, jarosite and iron oxides have also been described among the coastal clastic sediments of SW Australian lakes where

environmental conditions at the phreatic-vadose interface were similar to those existing at the Gorbea shoreline (McArthur et al., 1991; Benison and Bowen, 2015). Also, cement precipitation of jarosite under vadose conditions has been described for the Creede mining district where the distribution of alunite and jarosite was used to track the paleowater table evolution (Rye et al., 2000).

The isotopic compositions of sulfate ($\delta^{34}S_{VCDT}$ and $\delta^{18}O_{VSMOW}$) in the selenitic gypsum of the salt flats (Fig. 4) are inherited from the prior hydrothermal sulfates present in the catchment and were slightly increased by fractionation caused by precipitation ($\varepsilon^{34}S = 1.65 \pm 0.12‰$, Thode and Monster, 1965; $\varepsilon^{18}O = 3.6 \pm 0.9‰$, Lloyd, 1967). Although the 3.5 m-thick gypsum on the NE Gorbea margin likely records more local isotopic information from the eastern margin of the salt flat, the series is well preserved, which allows continuous information on the evolution of the gypsum filling of the salt flat to be obtained. The evolution of the isotopic composition of the sulfate in this gypsum series shows higher oxygen values in the lower cycle, which reflect the prolonged leaching mainly from hypogene sulfates that occurred during the lacustrine phase in the humid period prior to the massive precipitation of gypsum. The $\delta^{18}O_{VSMOW}$ values of the upper cycle, which are an average of 5‰ lower, reflect more recent mixing with supergene contributions (Magaritz et al., 1989) or with sulfate produced by the oxidation of native sulfur from the nearby Cerro Bayo paleosolfataras. No other sources of light sulfate are expected in the absence of recent thermal activity and in an area with apparently simple hydrology that is totally controlled by the topographic gradient. Variability in the upper cycle would be related to the mixing changes related to high-frequency paleohydrological (and paleoclimatic) fluctuations. The central selenites in the salt flat have lower $\delta^{34}S_{VCDT}$ and $\delta^{18}O_{VSMOW}$ values for sulfate and are similar to the upper ones in the northeastern margin outcrop. These lower isotopic compositions should be attributed to a greater contribution of light sulfate inputs coming from the oxidation of native sulfur (in Cerro Bayo and the eastern part of the Cordón de Azufre; Fig. 1a, b). Based on the hydrochemical and isotopic data, mixing by recycling through thermalism with old underground evaporites has been considered previously (Risacher and Fritz, 2000; Risacher et al., 2011) due to the presence of Upper Cretaceous-Paleogene and Neogene continental evaporites in the central Altiplano substrate (Alonso, 1991; Alonso et al., 1984). Risacher et al. (2011) propose, considering the Mg content and the $\delta^{34}S$ of the dissolved sulfate in thermal waters of northern Chile, the thermal dissolution and recycling of Cenozoic evaporitic formations located below the volcanoes. The comparison between the $\delta^{34}S_{VCDT}$ of the gypsum layer and its aluminum sulfate precursors (Table 3), with the continental evaporites and saline outcrops in the Central Andes (far lower on average, $\delta^{34}S_{VCDT} \approx +6‰$; Table 6, Fig. 7) suggests that there are local factors that influence the Gorbea area. This is also evident because alunite samples from the NW alteration zone in the Gorbea watershed have an average $\delta^{34}S_{VCDT} \approx +13‰$, whereas in the S alteration zone it is between +3 and + 4‰. In this case the high values in the NW zone could also be explained here by local recycling of the Upper Jurassic (Oxfordian) and Upper Cretaceous marine sulfates (64 Myr K-Ar age in a basaltic flow interleaved on top of the evaporitic series) that crop out in the Andean Precordillera (Hopper and Correa, 2000; $\delta^{34}S_{VCDT} \approx +15$ to +18.5‰, Claypool et al., 1980; Table 8 in Appendix). Nevertheless, the nature of the eastward extension of these evaporites, which mainly consist of anhydrite and crop out on the western flank of the Andean Precordillera, is unknown. The higher $\delta^{34}S_{VCDT}$ and $\delta^{18}O_{VSMOW}$ values for the gypsum layer for the Gorbea salt flat (+18‰ and + 24‰, on average; Table 3) are related to fractionation by precipitation (Thode and Monster, 1965; Lloyd, 1967) of the sulfate leached from the epithermal aluminum sulfates in the catchment.

4.3. Salar evolution and paleoclimatology

Supergene weathering began in the basin at the onset of thermalism in the Miocene, at 20 Ma, until approximately 13 Ma BP (Bissig and Riquelme, 2010). The end of the supergene weathering is consistent with the first hyper-arid phase that affected the Atacama Desert (s.l.), which has been dated between 12 and 8 Ma (Alpers and Brimhall, 1988; Rech et al., 2006, 2010, 2019). Thereafter, there were periods of extreme aridity, mostly between 6 and 3 Ma (Bissig and Riquelme, 2010) and between 9 ka BP and today. The latter arid Holocene phase included the mid-Holocene complex dry period, which was characterized by centennial-scale alternations of hyperarid and relatively humid periods (Paduano et al., 2003, Tapia et al., 2003, Grosjean et al., 2007, Giralt et al., 2008; Fig. 2). The last major humid phase took place in the Late Pleistocene between approximately 120 and 11 ka BP due to global climate causes (Tapia et al., 2003, Placzek et al., 2006; Fig. 2). It is mainly during this humid period that hypogenic and supergene sulfate minerals were leached towards the Gorbea and Ignorado paleolakes. The reactivation of thermalism in the late Pleistocene, for which there is great evidence in the nearby altiplanic setting as important travertine bodies and paleogeysers (Alonso and Viramonte, 1985; Alonso, 1991; Gibert et al., 2009), strongly contributed to the leaching. Regarding the bacterial activity, although continuous over time in low temperature conditions, it should have been much more intense in the humid periods of the Middle Miocene and the Pleistocene (Fig. 2). Supergene

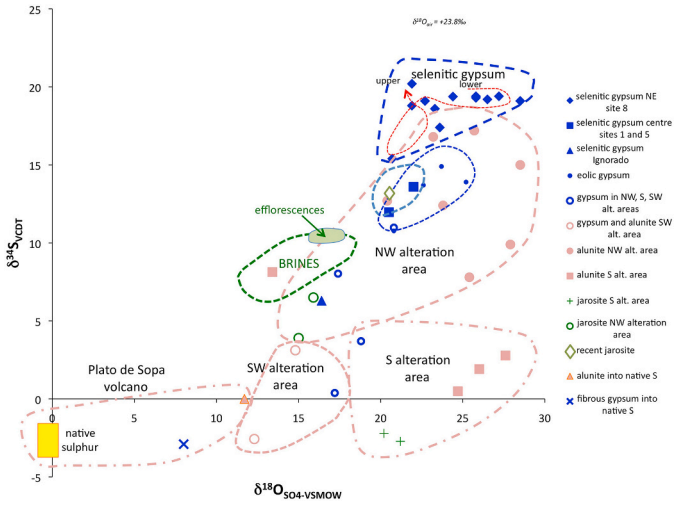

Fig. 4. $\delta^{34}S_{VCDT}$ and $\delta^{18}O_{SMOW}$ values for sulfate. The samples are grouped by lithology and emplacement. In addition to the solid samples, data from recent brines and efflorescences from the Gorbea salt flat are included.

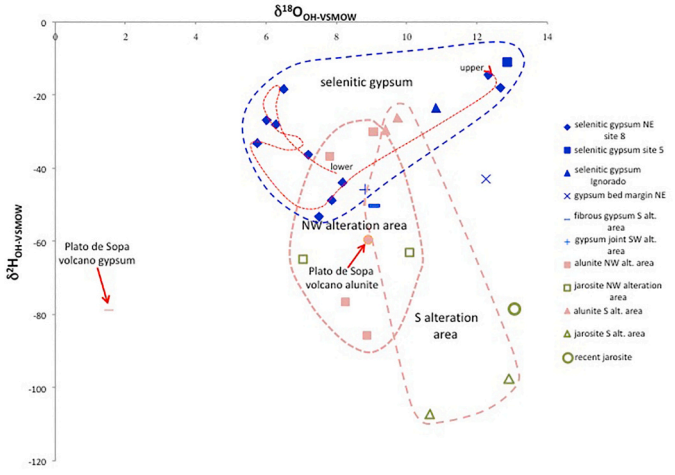

Fig. 5. $\delta^{2}H_{SMOW}$ and $\delta^{18}O_{SMOW}$ values for the crystallization water. The Gorbea salt flat samples are grouped by lithology and emplacement.

alteration, although it can happen in both oxic and anoxic environments, the latter case predominates volumetrically due to the rapid uptake of dissolved oxygen at depth by sulfide oxidation. The aerobic bacteria that could potentially intervene—if we consider the genera currently observed in sediments and brines—are *Sulfobacillus*, *Alicyclobacillus*, *Mycobacterium*, *Ralsonia*, *Burkholderia*, and *Marinobacter*. In anoxic environments the currently existing genera are *Desulfomicrobium* and *Clostridium* (Escudero et al., 2018), and their activity coexisted with the abiotic oxidation of the reduced sulfur species.

The very shallow nature of both paleolakes is shown by the absence of paleoshores. The presence of primary selenitic gypsum, which is a lithofacies whose crystals grew competitively from a decimeter-brine water column, reflects the development of a 'salina' environment prior to the definitive change to a salt flat. The age of the gypsum layer (6.37 ka BP; Table 5) broadly agrees with the beginning of the mid-Holocene complex dry period (7.5 to 4 cal ka BP). Considering a sedimentation rate of 0.37 $cm \cdot yr^{-1}$ for selenitic gypsum that has been measured in marine salt studies (Ortí et al., 1984), and assuming uninterrupted sedimentation, the time interval for gypsum precipitation in the Salar de Gorbea would be near 1 ka. Nevertheless, discontinuities in the gypsum layer as well as textural variations suggest that this 3.5-m-thick gypsum layer represents a longer sedimentation interval. Thus, during the mid-Holocene arid period, the Gorbea lake transitioned from a saline lake (≈ 7 ka BP) prior to the precipitation of the gypsum to a salina (≈ 6 to 5 ka) when selenitic gypsum precipitated, and finally to a salt flat (≈ 5 to 4 ka), when the gypsum layer was exposed to weathering. The gypsum layer was largely destroyed by dissolution, deflation, and neotectonics, between 4 ka BP and the present, during the relatively humid Holocene periods (Sáez et al., 2007; Pueyo et al., 2011). The OSL aliquots also show several age clusters that suggest the input of quartz grains during the short-lived relatively humid events that occurred over the last 4 kyr (at least at 3.4 ± 0.4, 2.5 ± 0.2 and 1.4 ± 0.1 ka). A short-lived humid period between 1 ka and 0.2 ka was responsible for the development of the recent ponds (Sáez et al., 2016) that are now surrounded by efflorescences. Similar dissolution events have been described for other altiplanic salt flats (Stoertz and Ericksen, 1974). In the Uyuni salt flat, they have been interpreted as representing the end of the dry period in the Altiplano at approximately 3 ka (Risacher and Fritz, 2000; Grosjean et al., 2007; Bao et al., 2015). Strong increases in salinity observed in fluid inclusions along selenitic gypsum crystals on the Ignorado salt flat were explained as the result of pulses of hydrothermal fluids (*saline ore fluids*) into the surface aquifer (Karmanocky and Benison, 2016). These pulses would be related to the existence of recent active magmatic inflation in this area detected by laser interferometry (Froger et al., 2007; Ruch and Walter, 2010). However, only the gypsum crystals that grow in the ponds would be suitable for measuring very recent weather events. Selenitic crystals of the old gypsum layer that covers the Gorbea salt flat are several thousand years old according to the OSL data and the available paleoclimatic information.

The paleoenvironmental evolution described above is consistent with the isotopic evolution of the compositional water of the selenitic gypsum found in the Gorbea salt flat. The δ^2H_{VSMOW} and $\delta^{18}O_{VSMOW}$ values in crystallization water of the gypsum layer of the northeast outcrop (Site 8, Fig. 1b) are lower in the basal cycle, which shows less evolved brines. The upper cycle shows a clear increase in both isotopic compositions, to more evolved brines. This fact confirms that the uppermost selenitic layers of the eastern outcrop are equivalent to those in the central part of the salt flat that also have the heaviest waters ($\delta^2H_{VSMOW} = -11‰$; $\delta^{18}O_{VSMOW} = +13‰$, Table 3). The high values of $\delta^{18}O_{VSMOW}$ in sulfate and low values in $\delta^{18}O_{VSMOW}$ in crystallization water occur because oxygen in sulfate retains the original signal of the thermal origin, whereas the hydration water reflects the degree of evaporation of the lake brines where gypsum precipitates from the recycled sulfate (Seal II et al., 2000). The supergene alteration that formed the hydrated sulfates around the salt flats took place in the wet periods after the formation of the sulfide deposits (mainly between 14 and 9 Ma and less developed between 120 and 9 ka BP; Fig. 2). The hydrology throughout the Miocene alteration phase cannot be accurately simulated, but in doing so from the Pleistocene until today, the compositional water (δ^2H_{VSMOW} and $\delta^{18}O_{VSMOW}$) of the hydrated sulfates fits fairly well to the expected field of the local hydrological evolution (Fig. 8).

4.4. Sulfate in the Atacama environment

Saline compounds and evaporites formed in continental areas usually come from nearby sources in the same watershed (Blatt et al., 1972), as external fluid inputs which can be deep-seated, or from atmospheric deposition, the latter being quantitatively significant in arid zones, as has been probed in the Atacama, Antarctica, and other deserts (Michalski et al., 2004; Lybrand et al., 2016). In areas without significant volcanic-thermal activity evaporitic sulfates are very often the

Table 4
Representative data from brines of the Gorbea and Ignorado salt flats.

Sample	Latitude	Longitude	T	pH	Salinity	Redox	Cl	SO_4	Na	K	Mg	Ca
			^oC		g/L	mV	mg/L	mg/L	mg/L	mg/L	mg/L	mg/L
Gorbea 1	S-25°25'43.1"	W-68°41'25.3"	11.6	3.44	80	382.6	26,980	21,695	12,660	380	6295	633
Gorbea 2	S-25°25'57.0"	W-68°41'08.6"		4.5	81		28,040	22,610	13,195	385	6565	660
Bofedal 3	S-25°29'29.9"	W-68°38'08.7"	16	3.9	17		5555	5510	2725	104	1320	496
Ignorado 4	S-25°29'58.2"	W-68°37'28.5"	15.8	3.59	10		980	4590	1220	230	480	457
Gorbea 5	S-25°25'25.2"	W-68°41'13.8"	8.7	2.67	216	285.6	96,730	48,570	39,010	2135	21,225	383
Gorbea 6	S-25°21'19.4"	W-68°38'24.6"	14	4.77	9		3145	1110	1970	107	36	412
Gorbea 7	S-25°24'10.7"	W-68°39'22.0"	5	2.35	34		10,255	10,400	5340	433	2255	491

Sample	Latitude	Longitude	Fe	Mn	Al	B	Si	Li	As	$\delta^{18}O$	δ^2H	$\delta^{34}S_{SO4}$	$\delta^{18}O_{SO4}$
			mg/L	mg/L	mg/L	mg/L	mg/L	mg/L	mg/L	‰	‰	‰	‰
Gorbea 1	S-25°25'43.1"	W-68°41'25.3"	23	113	1190	363	40	61	0.61	+1.63	−28.4	+9.0	+15.0
Gorbea 2	S-25°25'57.0"	W-68°41'08.6"	23	118	1235	380	41	62		+1.46	−24.5	+8.8	+15.8
Bofedal 3	S-25°29'29.9"	W-68°38'08.7"	4	23	225	76	33	12	0.27	−4.63	−51.6	+8.5	+14.6
Ignorado 4	S-25°29'58.2"	W-68°37'28.5"	2	6	86	19	52	2	0.22	+0.53	−25.5	+6.3	+13.2
Gorbea 5	S-25°25'25.2"	W-68°41'13.8"	<2	353	2170	953	13	218	1.29	−1.98	−12.3	+9.4	+15.2
Gorbea 6	S-25°21'19.4"	W-68°38'24.6"	<0.2	1	8	60	99	8	0.25	−0.46	−39.4	+7.5	+12.2
Gorbea 7	S-25°24'10.7"	W-68°39'22.0"	30	43	502	167	69	25	2.89	−2.53	−47.2	+9.3	+18.6

The upper table includes the physicochemical data and the concentrations of the major electrolytes, and the lower table shows the minor components and the isotopic compositions of water and dissolved sulfate.

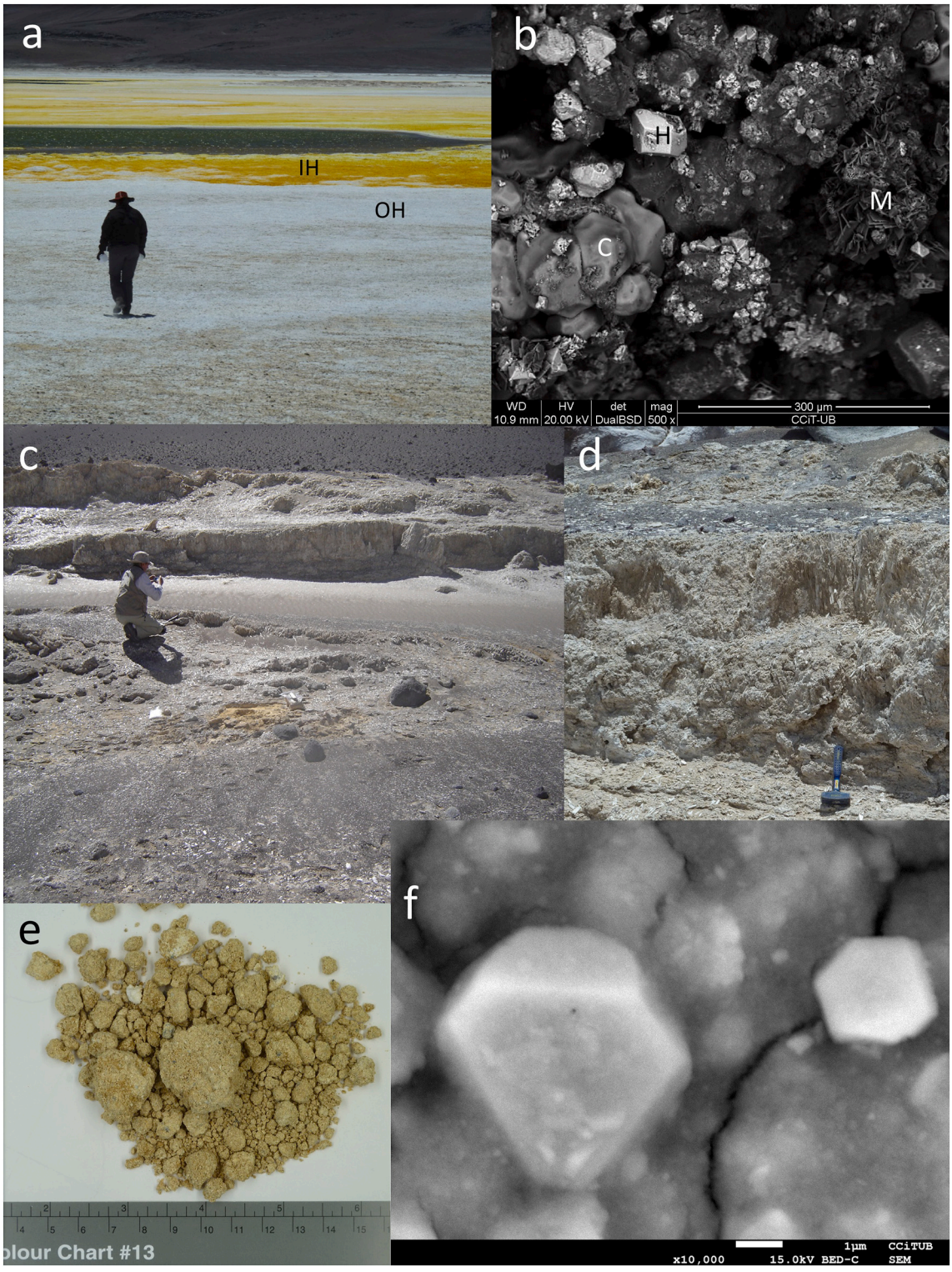

Fig. 6. Saline compounds in the salt flat. **a)** Efflorescences around the ponds. The inner halo (IH) close to the brines is yellowish because of the presence of minor amounts of Fe-bearing salts, whereas the outer halo (OH) is white. **b)** Detail of the inner efflorescences. The main minerals are hexahydrite (dark gray), carnallite (light gray-C), halite (white-H) and magnesioaubertite (tabular dark gray-M). SEM back-scatter electron microscopy image. **c)** Gypsum outcrop in NE margin of Gorbea salt flat (site 8 in Fig. 1). As on the salt flat surface, the old and inactive crust is composed of several levels of primary selenitic gypsum. **d)** Detail of the selenitic gypsum crust on the NE margin. **e)** Sand and gravel grains coated by recent jarosite a few meters from the western coast of the Gorbea salt flat. The color is greenish. **f)** Coating formed of euhedral micrometric jarosite that precipitated as cement. SEM back-scattered electron microscopy image.

Table 5
Seventeen of the aliquots met the SAR criteria and are shown here. The OSL age obtained from the average of the aliquots for the lower part of the gypsum, 1.1 m from the base, is 6.37 ± 0.67 ka BP. OSL dating was performed on 70 quartz aliquots obtained by dissolution of gypsum rock, as explained in the methodology.

Aliquot	Equivalent Dose	error	Dose Rate	error	Age	error
number	*Gy*		*Gy·ka^{-1}*		*ka*	
1	1.614	0.296	1.237	0.056	1.304	0.246
2	1.707	0.134			1.380	0.125
3	1.890	0.338			1.527	0.282
4	3.013	0.418			2.435	0.356
5	3.143	0.613			2.540	0.509
6	3.254	0.474			2.630	0.401
7	4.022	0.906			3.250	0.747
8	4.247	0.711			3.433	0.596
9	4.519	1.136			3.652	0.933
10	5.859	1.238			4.735	1.024
11	7.693	1.078			6.218	0.916
12	10.667	2.929			8.621	2.400
13	12.096	1.774			9.776	1.502
14	12.924	4.938			10.446	4.020
15	16.438	2.602			13.286	2.188
16	17.019	5.403			13.756	4.412
17	18.897	7.909			15.273	6.430

Aliquots	Age	error
	ka	*1σ*
1 to 3	1.391	0.104
4 to 5	2.529	0.236
6 to 8	3.429	0.418
9 to 17	6.373	0.672

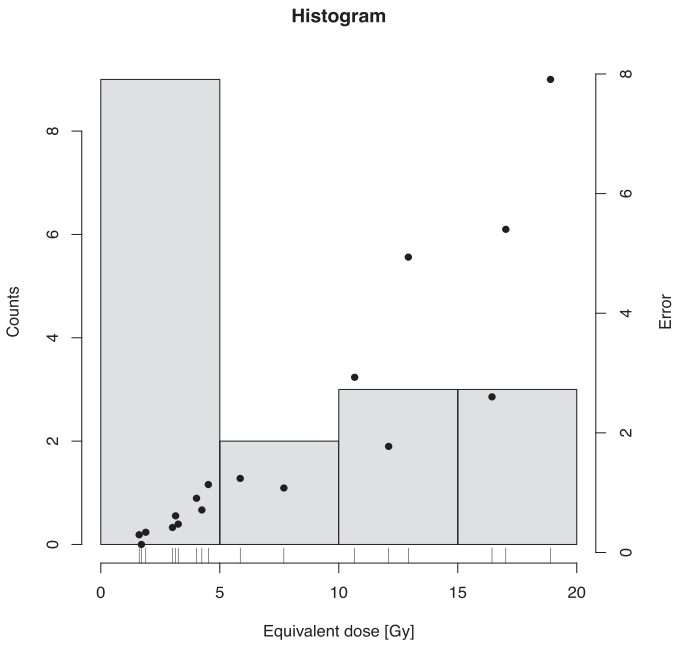

Table 6
$\delta^{34}S_{VCDT}$ and $\delta^{18}O_{VSMOW}$ values of sulfate samples from the arid Atacama area (Atacama Desert s.s. and Altiplano).

Isotopic composition of continental evaporitic sulfate (mostly gypsum) from the Central Andes				nr samples	$\delta^{34}S$	$\delta^{18}O$
Name	**Site**	**Coordinates**	**Age**			
Salar de Rio Grande	Altiplano	25°03'S 68°10'W	Neogene to Recent	13	+4.1	+13.4
Salar del Rincón	Altiplano	24°06'S 67°04'W	Neogene to Recent	14	+6.6	+12.8
Salar de Atacama	Atacama basin	23°36'S 68°14'W	Neogene to Recent	34	+7.6	+16.1
Cordillera de la Sal	Atacama basin	23°00'S 68°20'W*	Neogene	24	+4.8	+12.1
Hilaricos, Soledad, Lomas de la Sal	Central Depresion	21°22'S 69°20'W*	Neogene	38	+6.1	+13.8
Salar Grande	Coastal Range	20°53'S 70°00'W	Neogene	19	+7.2	+10.6
Pisagua gypsum	Coastal Range	19°35'S 70°12'W	Neogene	3	+6.8	+11.2
Mejillones gypsum	Coastal Range	23°19'S 70°26'W	Neogene	3	+4.7	+12.9

(*) *approximate coordinates in a wide area.*
Almost all of the data are average values; therefore, the geographic coordinates are approximate for large outcrops. Complementary and more detailed data are found in Table 8 - Appendix.

result of the recycling of older evaporites (Utrilla et al., 1992; Taberner et al., 2000; Cendón et al., 2004) or the oxidation of sedimentary sulfides exhumed by geodynamic causes (El Tabakh et al., 1997; Chivas et al., 1998).

The volcanic arc in the Andean area since the Cretaceous must be broadly considered to be one of the main sources of sulfate to approximately one hundred salt flats and to soils and saline dust of the Atacama Desert since the Miocene (Table 6; Pueyo et al., 2001; Rech et al., 2003). Magmatic-hydrothermal contributions, mainly from epithermal and porphyry copper deposits that spatially and temporally interacted with the external geological cycle, have been a major source of sulfate. Other contributions in the Andean arid area were from marine spray and coastal fog that can enter deep into the continent depending on topography (Rech et al., 2003), atmospheric deposition—such as what happens with nitrate (Böhlke et al., 1997) and sulfate (Bao et al., 2004)—and likely the local recycling of marine Mesozoic evaporites by thermal events in the Precordillera (Barton and Johnson, 1996; Hopper and Correa, 2000).

Continental salt basins filled with very pure halite, such as the Salar de Atacama (with more than 900 m thick saline sediments) or the Salar Grande (about 150 m thick in the depocenter), in the Atacama Desert s.l. have been explained by the selective recycling of saline compounds (mostly NaCl) from topographically higher (altiplanic) salt flats through the hydrological system (Chong et al., 1999; Rissmann et al., 2015). Recycling evidence is widespread in the continental evaporites of the Atacama Desert s.l. in space and time. The oldest continental evaporites in the area are in the Purilactis Fm. (≈ Paleocene; located in the Andean Precordillera and on the W margin of the Salar de Atacama basin), displaying low $\delta^{34}S_{VCDT}$ and $\delta^{18}O_{VSMOW}$ values, similar to those of sulfate leached from unaltered ignimbrites (Fig. 7). Younger evaporites, such as the Hilaricos, Soledad, Lomas de la Sal, and Rio Loa-Aduana gypsum (Tables 6 and 8 in Appendix; Figs. 1a and 7) have higher isotopic compositions. Continental Cenozoic evaporites in the Atacama Desert s.l. draw together a trend whose slope matches with the isotope enrichment of gypsum precipitation (Carmona et al., 2000). In recycling, the dissolution of old evaporites is carried out without isotopic fractionation since it consists of a process that advances without mass discrimination. Since the gypsum precipitated from the resulting brine is

Table 7
Isotopic enrichments ($\varepsilon^{18}O$, $\varepsilon^{34}S$) measured in laboratory experiments and sulfide leaching facilities.

Reference	$\varepsilon^{18}O_{SO4\text{-}H2O}$	Environmental conditions					Process
	‰	*Oxic*	*Anoxic*[b]	*Biotic*	*Abiotic*	*pH*	
Taylor et al., 1984	+4.5 to +6.2	x			x	7 to 1.6	Pyrite leaching
"	+8.9 to +10.9	x		x		7 to 1.6	"
Balci et al., 2012	+8.2		x	x		3[a]	Sphalerite leaching
"	+7.5		x		x	3[a]	"
"	+8.2	x		x		3[a]	S^o oxidation
"	+8.3	x			x	3[a]	"
Brabec et al., 2012	+5.6		x	x		7	Lab experiment
	$\varepsilon^{18}O_{SO4\text{-}O2}$						
Balci et al., 2007	−10.8	x		x		2.7	Pyrite leaching
"	−9.8	x			x	2.7	"
	$\varepsilon^{18}O_{SO3\text{-}H2O}$						
Müller et al.2013a,b	+37		x		x	1.5	Lab experiment
"	+15.2		x		x	6.3 to 9.7	"
	$\varepsilon^{34}S_{SO4\text{-}S2\text{-}}$						
Alam et al., 2013	(−5.8[1]) +1.8		Tetrathionate	x		7	Lab experiment
Brunner et al. 2008[c]	≈ 0			x		2[a]	Lab experiment
Balci et al., 2007	−0.7		x	x	x	3[a]	Pyrite leaching
Balci et al., 2012	≈ 0	x		x	x	3[a]	Sphalerite leaching
"	−2.6[d]		x	x	x	3[a]	S^o oxidation
Balci et al., 2017	−0.9	x		x		4[a]	

[a] Initial values (pH can strongly decrease during the experiment).
[b] Oxidation in anoxic environment was commonly performed using Fe^{3+}.
[c] Only S fractionation in case of SO_2 degassing at very low pH.
[d] Probably due to accumulation of intermediate sulfur compounds not totally oxidized.

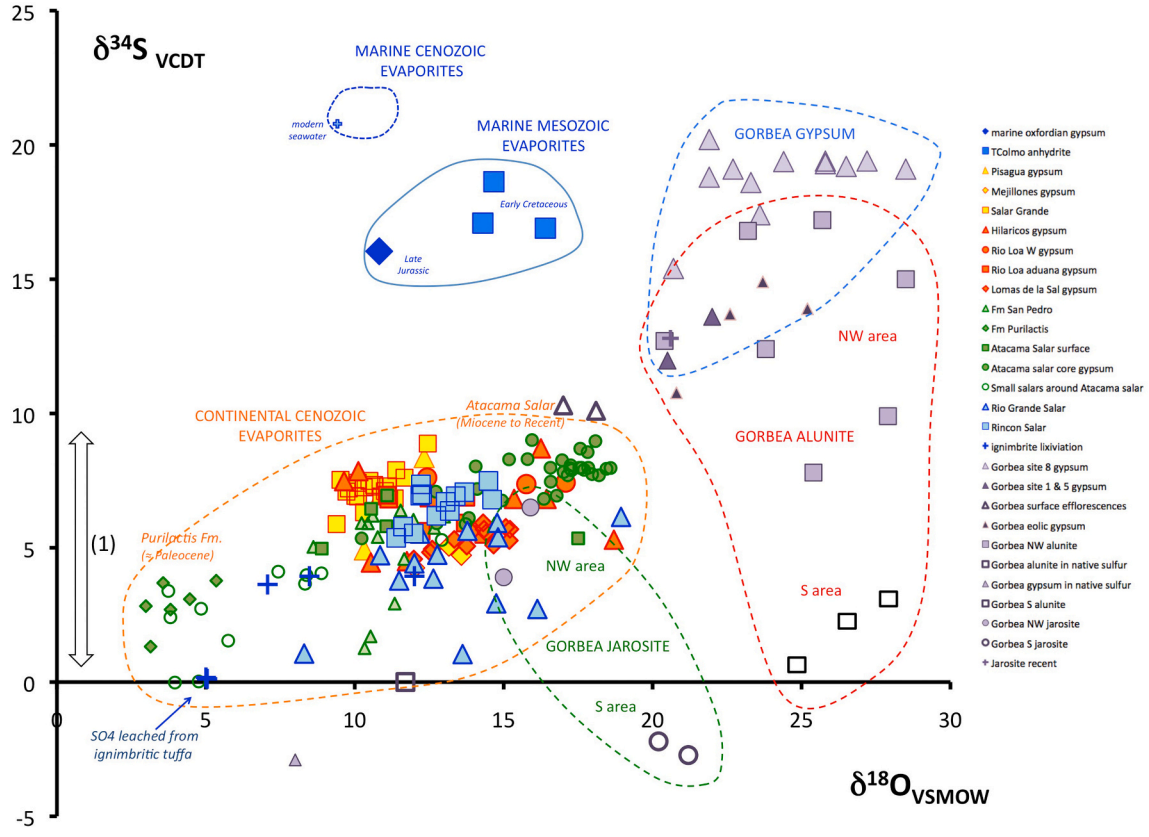

Fig. 7. Comparison of the isotopic compositions ($\delta^{18}O_{VSMOW}$, $\delta^{34}S_{VCDT}$) of sulfate in the Gorbea salt flat basin and the evaporitic sulfates from the Atacama Desert s.l. Arrow (1) shows the range of $\delta^{34}S_{VCDT}$ values previously reported for evaporitic and edaphic sulfates present in the Atacama Desert (Spiro and Chong, 1996; Böhlke et al., 1997; Pueyo et al., 2001; Rech et al., 2003; Leybourne and Cameron, 2006; Leybourne et al., 2013; Rissmann et al., 2015).

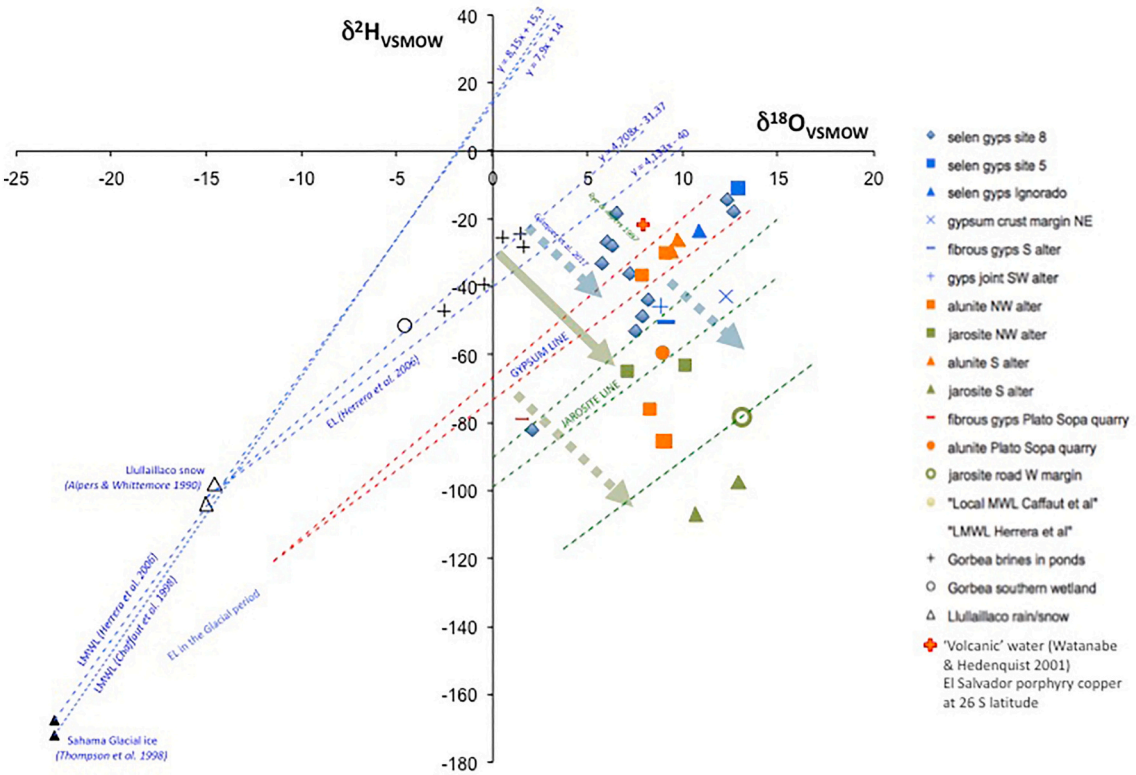

Fig. 8. Two local meteoric water lines (LMWL) obtained at the Quisquiro salt flat (N Chile at 23°16′S latitude, 4200 m altitude, Chaffaut et al., 1998) and on Lake Chungará (N Chile at 18°14′ S latitude, 4000 m altitude, Herrera et al., 2006); two evaporation lines (EL) (Herrera et al., 2006) are also represented. The 'gypsum and jarosite lines' were calculated considering the respective enrichments with respect to the brine for $\varepsilon^{2}H$ and $\varepsilon^{18}O$ at room temperature (Gázquez et al., 2017, for gypsum; Rye and Alpers, 1997, for jarosite). The meteoric water for the Glacial period (about $\delta^{18}O_{SMOW}$ 6‰ lower than that of the Holocene) has been approximated from ice cores taken from the Nevado de Sahama (Thompson et al., 1998). Isotopic data of local precipitation are known by snow analysis of the Llullaillaco volcano (Alpers and Brimhall, 1988).

isotopically heavier than the dissolved sulfate, the repetition throughout the hydrological cycle of this process in successively younger basins results in the trend towards progressively higher $\delta^{18}O$ and $\delta^{34}S$ values in the resulting gypsum (Thode and Monster, 1965; Lloyd, 1967). The preferred recycling of NaCl and other very soluble compounds, with respect to sulfate, can take two forms: i) selective dissolution of the already precipitated soluble compounds caused by unsaturated groundwater; and ii) chemical brine fractionation by precipitation of the most insoluble compounds (such as sulfate), followed by brine leakage to the hydrological system. Previous works involve deep brines in the genesis of the Cenozoic evaporites and nitrate deposits in the Atacama Desert (Rech et al., 2003; Risacher et al., 2003; Leybourne and Cameron, 2006; Leybourne et al., 2013; Rissmann et al., 2015; Godfrey and Alvarez-Amado, 2020). These brines, present in deep aquifers and circulating along fractures, are the result of the recycling of altiplanic waters and brines and their mixing with the aforementioned sources of saline compounds. Available quantitative data on these sulfate sources are: i) the marine aerosol inputs can, in some exposed places (where the Cordillera de la Costa has been eroded), reach up to 50% of the total sulfate, quickly damping down to 90 km inland (Rech et al., 2003); ii) the amount of atmospheric sulfate, calculated from its ^{17}O content, seems to reach about 9%, with local values up to 24% of the total sulfate in the central part of the Atacama Desert (Bao et al., 2004); iii) the possible recycling of marine evaporites from the Mesozoic, which crop out in the Precordillera, has not yet been measured, but given the aridity during the Cenozoic, it should only have a limited scope. Therefore we must conclude, given the previous considerations, that the magmatic-hydrothermal processes that occurred between the W margin of the Andean Ranges and the Pacific Ocean, since the development of the Middle Cenozoic magmatic arc, are one of the main first sources of the sulfate content in the Atacama Desert and related areas (Salar de Atacama, Spiro and Chong, 1996, Carmona et al., 2000; Chilean Central Depression, Pueyo et al., 2001; Atacama Desert soils, Rech et al., 2003; and other places in the Atacama Desert s.l., Table 6). Due to the general aridity, with two hyper-arid phases between the Late Miocene and the Present (Fig. 2) and the endorheic character of a large part of the area, the drainage has not been enough to remove the soluble salts produced throughout this period.

The area surrounding Gorbea is a suitable place to show the local recycling of sulfur compounds and their interplay between the internal and external geological cycles. The $\delta^{34}S_{VCDT}$, $\delta^{18}O_{VSMOW}$, $\delta^{2}H_{VSMOW}$ data from sulfates are compared with those from other sites of the Atacama Desert (soils, saline formations, brines) to find relationships and provenances. The hydration water of sulfates, either H_2O or OH, allows knowing the hydrological context in which sulfate recycling occurs between the magmatic-thermally altered country rocks and salt flats. The Atacama Desert s.l. is a complex environment were diverse contributions intervene, but the main sulfur input is magmatic in several forms.

A recent source of interest in the matter derives from data obtained on the surface of Mars by remote sensing and surface probes. The presence of saline materials with acid sulfate assemblages, including jarosite and magnesium salts, was recognized by the CRISM (Compact Reconnaissance Imaging Spectrometer for Mars) in Noctis Labyrinthus (Thollot et al., 2012). The presence and preservation of these mineral assemblages in the Gorbea setting, where jarosite precipitates around and inside the salt flat as pore cements and efflorescences with other neutral and acid salts of Fe and Al, makes this environment a geological,

environmental, and possibly a microbiological analogue (Davis-Belmar et al., 2013; Benison and Karmanocky III, 2014; Benison, 2019), of the conditions that might have existed in the Middle Permian and other periods on Earth (Long and Lyons, 1992; Benison et al., 1998; Benison and Bowen, 2013, 2015) and perhaps on Mars in the Theiikian era, which was equivalent to the Archaean on Earth (Benison, 2006; Benison and Bowen, 2006; Bibring et al., 2006).

5. Conclusions

The acidic brines in ponds located in the topographically lower parts of the Gorbea salt flat give rise to efflorescences formed by acid paragenesis. The efflorescences are composed of minerals containing aluminum and iron (Mg-aubertite and hydroxysulfates) and common evaporitic minerals (halite, thenardite, hexahydrite). The topographically higher and older parts of the salt flat consist of a partially destroyed selenitic gypsum crust. The predominance of sulfates in the Gorbea salt flat—rather than chlorides, which are much more common in the altiplanic salt flats—is related to recycling by leaching of native sulfur and other sulfate compounds (alunite, jarosite, anhydrite, and gypsum) associated with epithermal bodies and volcanic edifices in the watershed. The predominance of sulfates occurs in other similar sites, such as the Salar de Rio Grande (Argentine Altiplano), where thenardite is the main mineral.

The isotopic compositions ($\delta^{34}S_{VCDT}$, $\delta^{18}O_{VSMOW}$) of the epithermal sulfates have wide distributions in the Gorbea watershed due to mixing of hypogene and supergene provenances. The highest values of $\delta^{34}S_{VCDT}$ and $\delta^{18}O_{VSMOW}$, which are found in the selenitic gypsum crust of the salt flat, indicate that the recycling occurred locally and was mainly from the isotopically heavy hypogene sulfates. The $\delta^{18}O_{VSMOW}$ (and less clearly, the $\delta^{34}S_{VCDT}$) values are higher in the lower part of the gypsum crust, suggesting an initial and dominant hypogene signature in the waters of the earlier paleolake, that decreases towards the top, probably due to mixing with more recent supergene inputs during gypsum precipitation. Bacterial processes were more active during the supergene phases and have remained residual to this day; they do not seem to have had a significant influence on the isotopic composition of the sulfate. The low environmental pH, which increases the activity of sulfite species, has been much more determinant of some scattering of the $\delta^{18}O_{VSMOW}$ values due to isotopic exchange with water or with dissolved oxygen. The crystallization water of the gypsum ($\delta^{18}O_{VSMOW}$) is lighter in the basal part of the selenitic crust, which still represents few evolved brines; it became progressively heavier towards the upper part and towards the center of the salt flat prior to the final drying at approximately 4 ka BP. The main sulfate recycling in the salt flat basin occurred during the last humid Pleistocene period that ended with CAPE II (about 10 ka BP) in the central Atacama (Fig. 2).

The values found in the watershed and in the Gorbea and Ignorado salt flats are different from those generally found in the Atacama Desert (*s.l.*) where the $\delta^{34}S_{VCDT}$ and $\delta^{18}O_{VSMOW}$ values are generally between +4 and + 8‰ and between +10 and + 18‰, respectively. This difference is due to the fact that evaporitic sulfate in the Gorbea salt flat mostly came from direct recycling of epithermal sulfates mixed with S^0 oxidation products, while sulfate of soils and evaporites in the Atacama Desert s.l. also reflect other contributions—in space as well as in time. The main source of sulfate is the oxidation of sulfides and other magmatic-hydrothermal compounds, mixed with atmospheric deposition, contribution of leaked brines, local recycling of old evaporites, and near the coast, marine aerosols. East to west transport of some of these contributions occurs through the hydrologic system, whose main recharge area is located in the Altiplano, with a height difference of up to 3000 m with respect to the Central Depression. The importance of brine leaks of the altiplanic salt flats and the recycling of old evaporites is also demonstrated by the fact that Cenozoic evaporites located west of the Altiplano are, in general, richer in chlorides than the altiplanic ones.

Declaration of Competing Interest

None.

Acknowledgments

Three campaigns (2011, 2012 and 2017) were funded by the FONDECYT Project number: 1100795 '*Microbial transformations of arsenic in saline environments in Northern Chile*' and '*Map of microbial diversity of Northern Chile*', BHP Minerals Americas (32002137). Complementary help was obtained thanks to the initiation FONDECYT project 11150686. The OSL dating was performed at the Institute of Geology of the University of A Coruña thanks to the '*Redes de Investigación*' project (R2017/008) of the Xunta de Galicia. The rest of analyses (XRD, SEM, isotopes) were made in the CCiT of the University of Barcelona and funded by the FBG project 000621. The text has been improved thanks to the kind reviews of Matthew Leybourne and another anonymous reviewer. We also thank Ricardo Alonso (UNSa), Carlos Ayora (CSIC) and Alberto Sáez and Angels Canals (UB) for their help in some aspects of the work. English editing by Grant George Buffett (www.terranova.barcelona), Earth scientist and native English speaker.

Appendix A

Table 8
$\delta^{34}S_{VCDT}$ and $\delta^{18}O_{VSMOW}$ data obtained in outcrops and cores from the Andean Altiplano to the Cordillera de la Costa, between 19 and 27° S latitude.

Sample	Latitude	Longitude	$\delta^{34}S_{VCDT}$	$\delta^{18}O_{VSMOW}$
Oxfordian gypsum				
YS	S 24° 44′ 01.0"	W 69° 09′ 04.3"	+16.04	+10.82
Teresa de Colmo. Upper Cretaceous anhydrite				
CBD11-314.8 m *[borehole/depth]*	S 25° 55′ 52.3"	W 70° 03′ 17.6"	+18.63	+14.67
CBD11-365.8 m	"	"	+16.90	+16.40
CBD12-402.7 m	"	"	+17.09	+14.30
Pisagua gypsum				
PI-1	S 19° 34′ 33.8"	W 70° 12′ 01.4"	+7.09	+10.91
PI-3	"	"	+4.92	+10.32
PI-8	"	"	+8.36	+12.33
Península Mejillones gypsum				
PM-2	S 23° 19′ 18.0"	W 70° 28′ 35.8"	+4.72	+13.58
PM-4	"	"	+5.06	+13.16
PM-6	"	"	+4.25	+12.01
Salar Grande (Loberas open) accessory sulfate				
5.1 m depth (top)	S 20° 53′ 29.6"	W 70° 01′ 26.4"	+8.88	+12.45

(*continued on next page*)

Table 8 (*continued*)

Sample	Latitude	Longitude	$\delta^{34}S_{VCDT}$	$\delta^{18}O_{VSMOW}$
8.8 m	“	“	+7.53	+9.52
13.5 m	“	“	+7.21	+9.80
15.7 m	“	“	+6.91	+10.11
17.4 m	“	“	+7.42	+10.10
18.0 m	“	“	+7.09	+9.72
22.6 m	“	“	+5.88	+9.39
25.0 m	“	“	+7.29	+11.12
26.5 m	“	“	+7.89	+11.39
28.0 m	“	“	+6.84	11.34
29.2 m	“	“	+7.61	+11.67
31.7 m	“	“	+7.28	+10.67
32.6 m	“	“	+6.32	+10.31
34.9 m	“	“	+7.34	+10.65
35.9 m	“	“	+6.91	+10.89
39.2 m	“	“	+7.49	+10.49
41.4 m	“	“	+7.11	+11.01
42.1 m	“	“	+7.25	+10.30
44.3 m (lowermost part o fthe open)	“	“	+6.93	+10.02
Hilaricos, Soledad gypsum				
q1.1	S 21° 32′ 56.4”	W 69° 38′ 12.0”	+4.50	+11.75
q1.2	“	“	+4.45	+10.54
Hilaricos				
hi22	S 21° 27′ 05.5”	W 69° 35′ 52.1”	+6.82	+16.44
hi23	“	“	+5.30	+18.70
hi25	“	“	+7.48	+9.64
hi25	“	“	+7.85	+10.12
hi29	“	“	+6.82	+15.35
hi27	“	“	+8.70	+16.25
Rio Loa W				
qw43	S 21° 28′ 03.1”	W 69° 43′ 19.6”	+7.61	+12.43
qw47	“	“	+7.43	+17.08
qw50	“	“	+7.37	+15.76
Rio Loa aduana Quillagua				
rl60	S 21° 37′ 36.2”	W 69° 32′ 55.3”	+5.92	+13.71
rl61	“	“	+5.61	+12.23
rl66	“	“	+5.50	+14.33
Llamara ponds gypsum				
ll52	S 21° 16′ 08.6”	W 69° 37′ 37.5”	+6.96	+11.09
ll55.2	“	“	+6.88	+13.73
ll54	“	“	+6.81	+11.14
ll54ext	“	“	+6.85	+12.49
Cerro Soledad				
cs30	S 21° 15′ 25.4”	W 69° 33′ 20.1”	+5.72	+15.02
cs31	“	“	+4.65	+15.15
cs32	“	“	+6.93	+11.05
cs33	“	“	+6.41	+14.21
cs34	“	“	+6.19	+16.19
cs35	“	“	+5.67	+13.88
cs36	“	“	+7.25	+13.51
Lomas de la Sal				
ls7.1	S 21° 22′ 00.1”	W 69° 26′ 48.5”	+5.06	+13.76
ls8	“	“	+5.93	+14.31
ls13	“	“	+5.10	+14.66
ls16	“	“	+4.83	+12.54
ls17	“	“	+4.95	+12.60
ls18	“	“	+4.58	+11.98
ls39	“	“	+5.27	+15.19
ls39.2	“	“	+5.31	+13.34
ls40gris	“	“	+5.59	+13.92
ls40bco	“	“	+5.76	+15.07
ls42	“	“	+5.69	+14.34
ls42	“	“	+5.69	+15.21
ls42.2	“	“	+5.56	+14.41
Salar Rio Grande				
SRG-2	S 25° 02′ 45.0”	W 68° 09′ 33.7”	+4.72	+10.85
SRG-4	“	“	+5.63	+13.78
SRG-12.1	“	“	+2.93	+14.75
SRG-12.3	“	“	+3.85	+12.64
SRG-13	“	“	+6.15	+18.94
SRG-15	“	“	+5.93	+14.78
SRG-16	“	“	+4.74	+12.77
SRG-19	“	“	+1.06	+8.30
SRG-21	“	“	+5.39	+14.81
SRG-23	“	“	+3.78	+11.49
SRG-26	“	“	+4.42	+12.00
SRG-28	“	“	+2.72	+16.13

(*continued on next page*)

Table 8 (*continued*)

Sample	Latitude	Longitude	$\delta^{34}S_{VCDT}$	$\delta^{18}O_{VSMOW}$
SRG-32	“	“	+5.53	+12.19
Purilactis series				
pur1	S 23° 40′ 00.1”	W 68° 40′ 37.0”	+2.83	+2.99
pur2	“	“	+2.70	+3.81
pur3	“	“	+3.09	+4.46
pur4	“	“	+3.77	+5.35
pur5	“	“	+3.69	+3.57
pur6	“	“	+1.32	+3.14
San Pedro Fm				
Cuchabrache, F.S.Pedro	S 22° 50′ 51.1”	W 68° 12′ 57.1”	+4.58	+11.66
Río Grande village, F. S. Pedro	S 22° 38′ 37.5”	W 68° 09′ 44.0”	+5.74	+12.67
Valle de la Luna	S 22° 56′ 20.1”	W 68° 16′ 42.1”	+1.70	+10.53
Valle de la Luna	S 22° 56′ 20.2”	W 68° 16′ 59.6”	+1.26	+10.33
Gypscreta Chulacao (V. Luna)	S 22° 55′ 20.1”	W 68° 14′ 13.0”	+2.92	+11.34
Displacive gypsum, southern part Cordillera de la Sal	S 23° 45′ 28.2”	W 68° 35′ 18.9”	+5.40	+10.77
Geoda gypsum, southern part Cordillera de la Sa	“	“	+6.04	+11.97
Gypsarenite, southern part Cordillera de la Sa	“	“	+5.92	+10.23
Rosett gypsum cata electric towers, Llano de la Paciencia	S 23° 32′ 27.4”	W 68° 33′ 30.7”	+5.03	+8.61
Selenític gypsum domes, path electric towers, Llano de la Paciencia	S 23° 33′ 09.3”	W 68° 33′ 48.7”	+5.91	+10.44
Anhydrite flat nodule, Quebrada path electric towers, Llano de la Paciencia	S 23° 34′ 40.4”	W 68° 34′ 28.6”	+6.19	+10.60
Fm San Pedro gypsum, northern part Llano de la Paciencia	S 23° 33′ 34.6”	W 68° 35′ 45.0”	+6.39	+11.54
Gypsum between salt, northern part Llano de la Paciencia	S 23° 30′ 48.6”	W 68° 34′ 44.8”	+6.16	+13.00
Atacama salt flat surface				
Southern lagoon sediment, Atacama saalt flat nucleus, R144	S 23° 42′ 47.0”	W 68° 16′ 03.1”	+5.35	+17.50
Quebrada Lila (near Tilopozo) sulfate 00–57	S 23° 47′ 41.6”	W 68° 16′ 31.1”	+5.80	+11.06
Sulfate crust, Small Salt flat, Llano de la Paciencia R156	S 23° 10′ 25.7”	W 68° 11′ 54.0”	+6.95	+11.09
Anhydrite flat nodule, Small Salt flat, Llano de la Paciencia R157	“	“	+6.45	+10.55
Sulfate in salt crust, Small Salt flat, Llano de la Paciencia R172	S 23° 09′ 56.8”	W 68° 30′ 42.0”	+4.97	+8.89
Atacama salt flat (core samples) [borehole/depth]				
2001/19 m	S 23° 34′ 24.0”	W 68° 23′ 27.9”	+6.11	+13.83
2001/19.91 m	“	“	+7.09	+13.63
2001/19.92 m	“	“	+5.88	+13.72
2001/35.3 m	“	“	+5.91	+12.75
2001/59.46 m	“	“	+8.03	+14.06
2102/48.6 m	S 23° 40′ 35.9”	W 68° 18′ 52.7”	+6.76	+14.94
2102/70.5 m	“	“	+5.35	+10.23
2023/12 m	S 23° 19′ 34.8”	W 68° 18′ 43.5”	+7.74	+17.97
2023/27.2 m	“	“	+7.90	+17.70
2034/16.85 m	S 23° 40′ 13.8”	W 68° 28′ 42.0”	+7.09	+12.72
2002/AT-15/47.3 m	S 23° 26′ 53.7”	W 68° 20′ 16.6”	+8.26	+16.96
2002/AT-21/71.4 m	“	“	+7.98	+17.54
2002/AT-27 (1 + 2)/99.7 m	“	“	+7.70	+17.15
2002/AT-42 (1)/196.75 m	“	“	+8.97	+18.08
2002/AT-51 (1)/248.05 m	“	“	+8.56	+17.82
2002/AT-60 (1)/282.1 m	“	“	+7.98	+17.61
2002/AT-64/308.2 m	“	“	+7.19	+14.11
2002/AT-66(2)/315.18 m	“	“	+7.82	+17.01
2002/AT-83 (1)/454.4 m	“	“	+7.53	+14.40
2002/AT-90/463.1 m	“	“	+8.30	+15.80
2002/AT-95 d (1)/476.73 m	“	“	+7.98	+16.57
2002/AT-96 c (1)/478.3 m	“	“	+8.69	+17.57
2002/AT-96 c (2)/478.34 m	“	“	+7.96	+17.23
2002/AT-98 (4)/484.65 m	“	“	+8.29	+15.18
2002/AT-86/489.08 m	“	“	+9.01	+15.95
2021/21.92 m	S 23° 20′ 59.7”	W 68° 16′ 57.0”	+7.89	+17.28
2021/24.4 m	“	“	+6.82	+16.35
2021/24.41 m	“	“	+6.94	+16.78
2021/40.9 m	“	“	+8.07	+17.25
2021/44.4 m	“	“	+7.94	+18.45
2021/100.3 m	“	“	+7.70	+18.20
2106/26.2 m	S 23° 33′ 48.8”	W 68° 09′ 43.1”	+7.46	+16.58
2106/116.3 m	“	“	+7.97	+18.59
2106/223.2 m	“	“	+7.98	+17.84
Small salt flat (west of Atacama salt flat)				
Gypsarenite (eolic), Elvira salt flat	S 23° 31′ 40.2”	W 68° 55′ 57.0”	−0.02	+3.96
Efflorescence in Qhebrada between Mariposa sand Los Morros salt flats	S 23° 45′ 57.1”	W 68° 57′ 00.4”	+0.02	+4.76
Salt crust, Verónica salt flat	S 23° 53′ 41.8”	W 68° 57′ 40.8”	+2.41	+3.81
Guipsum in piedmont, Mariposas salt flat	S 23° 53′ 34.0”	W 68° 47′ 34.3”	+4.11	+7.43
Guipsum in piedmont, Mariposas salt flat	S 23° 53′ 33.9”	W 68° 47′ 34.3”	+4.05	+8.88
Eflor.Q^{a}que va de Mariposas a Los Morros salt flats	S 23° 41′ 27.9”	W 68° 56′ 20.6”	+3.98	+8.38
Sulfate patinain ore sample, Sierra Mariposas	S 23° 44′ 04.8”	W 68° 53′ 39.8”	+3.39	+3.74
Efflorescence in Qhebrada between Mariposa sand Los Morros salt flats	S 23° 46′ 31.4”	W 68° 58′ 15.4”	+2.73	+4.84
Salt crust, Los Morrossalt flat	S 23° 40′ 19.6”	W 68° 57′ 13.6”	+3.66	+8.33
Gypsum in hills near Elvira salt flat	S 23° 30′ 32.7”	W 68° 57′ 12.1”	+1.54	+5.75
Altiplanic salt flats				
Salt crust,Aguas Calientes salt flat (southern part)	S 23° 54′ 56.2”	W 67° 39′ 48.8”	+5.29	+12.92

(*continued on next page*)

Table 8 (*continued*)

Sample	Latitude	Longitude	$\delta^{34}S_{VCDT}$	$\delta^{18}O_{VSMOW}$
Salar Rincón (R-8 borehole)				
3 m depth	S 24° 06′ 36.0”	W 67° 01′ 27.0”	+6.99	+12.26
5 m	“	“	+7.07	+13.68
20 m	“	“	+7.36	+12.22
30 m	“	“	+6.79	+14.61
48 m	“	“	+6.94	+12.20
54 m	“	“	+5.79	+11.62
60 m	“	“	+5.37	+11.39
78 m	“	“	+6.19	+12.74
85 m	“	“	+6.37	+13.19
91 m	“	“	+6.92	+13.39
103 m (a)	“	“	+5.53	+11.98
103 m (b)	“	“	+6.71	+13.05
111 m depth	“	“	+7.49	+14.49
Ignimbritic tuffa (leached SO_4)				
Not weathered	S 23° 11′ 37.3”	W 67° 59′ 30.8”	+0.17	+5.00
Weathered	“	“	+3.63	+7.07
Not weathered	“	“	+0.12	+5.04
Weathered	“	“	+3.94	+12.00
Weathered	“	“	+3.94	+8.48

Among the different sulfate samples included in the table some correspond to ancient salt flats between the Miocene and Pleistocene, as is the case of Hilaricos Unit, Soledad Fm, Lomas de la Sal, Salar de Llamara, Salar Grande, Salar de Atacama, Salar de Rio Grande, Salar del Rincón (the two last in the Puna Argentina). In addition, samples from older formations with sulfate content (Oxfordian and Upper Cretaceous marine evaporites cropping out in the Precordillera; Upper Cretaceous to Lower Eocene Purilactis Fm., and Oligocene to Lower Miocene San Pedro Fm) are also added.

References

Africano, F., Bernard, A., 2000. Acid alteration in the fumarolic environment of Usu volcano, Hokkaido, Japan. J. Volcanol. Geotherm. Res. 97, 475–495.

Aguilera, F., Layana, S., Rodríguez-Díaz, A., González, C., Cortés, J., Inostroza, M., 2016. Hydrothermal alteration, fumarolic deposits and fluids from Lastarria Volcanic complex: a multidisciplinary study. Andean Geol. 43 (2), 166–196.

Alam, M., Pyne, P., Mazumdar, A., Peketi, A., Ghosh, W., 2013. Kinetic enrichment of ^{34}S during Proteobacterial thiosulfate oxidation and the conserved role of SoxB in S-S bond breaking. Appl. Environ. Microbiol. 79 (14), 4455–4464.

Alonso, R., 1991. Evaporitas neógenas en los Andes Centrales. In: *Génesis de Formaciones Evaporíticas. Modelos Andinos e Ibéricos* (J.J. Pueyo, coord.). Publicacions Universitat de Barcelona, pp. 268–329. Estudi General 2. (417 pp).

Alonso, R., Viramonte, J., 1985. Geyseres Boratíferos de la Puna Argentina. *IV Congreso Geológico Chileno (Antofagasta)*, Actas II, pp. 23–44.

Alonso, R., Viramonte, J., 1987. Geología y metalogenia de la Puna. Estud. Geol. 43, 393–407.

Alonso, R., Gutierrez, R., Viramonte, J.G., 1984. Megacuerpos Salinos Cenozoicos de La Puna Argentina. *Actas del IX° Congreso Geológico Argentino*, I, pp. 25–41.

Alonso, R., Seggiaro, R., Palaci, C., 1985. Hallazgo de restos vegetales fósiles en cenizas volcánicas neoterciarias de la Puna jujeña. *XX Jornadas Argentinas de Botánica*, p. 57 (Salta).

Alonso, R.N., Jordan, T.E., Tabbutt, K., Vandervoort, D., 1991. Giant evaporite belts of the Neogene Central Andes. Geology 19, 401–404.

Alpers, Ch.N., Brimhall, G.H., 1988. Middle Miocene climatic change in the Atacama Desert, northern Chile: evidence from supergene mineralization at La Escondida. Geol. Soc. Am. Bull. 100, 1640–1656.

Alpers, Ch.N., Rye, R.O., Nordstrom, D.K., White, L.D., King, B., 1992. Chemical, crystallographic and stable isotopic properties of alunite and jarosite from acid-hypersaline Australian lakes. In: Lyons, W.B., Long, D.T., Herczeg, A.L., Hines, M.E. (Eds.), The Geochemistry of Acid Groundwater Systems, Chemical Geology, 96, pp. 203–226.

Arancibia, G., Matthews, S.J., Pérez de Arce, C., 2006. K-Ar and $^{40}Ar/^{39}Ar$ geochronology of supergene processes in the Atacama Desert, Northern Chile: tectonic and climatic relations. J. Geol. Soc. Lond. 163, 107–118.

Aravena, R., Suzuki, O., Peña, H., Pollastri, A., Fuenzalida, H.A., Grilli, A., 1999. Isotopic composition and origin of precipitation in Northern Chile. Appl. Geochem. 14, 411–422.

Arbiol, C., Rosell, L., Playà, E., 2014. Isotopic composition of the water of crystallization of gypsum as a tool for genetic interpretation: application to the Vilobí Gypsum Unit (Miocene, Barcelona). In: *19th International Sedimentological* Congress, 2014 18-22 August Geneva, Switzerland, p. 29.

Aubrey, A., Cleaves, H.J., Chalmers, J.H., Skelley, A.M., Mathies, R.A., Grunthaner, F.J., Ehrenfreund, P., Bada, J.L., 2006. Sulfate minerals and organic compounds on Mars. Geol. Soc. Am. 34 (5), 357–360.

Ayora, C., Caraballo, M.A., Macias, F., Rotting, T.S., Carrera, J., Nieto, J.M., 2013. Acid mine drainage in the Iberian Pyrite Belt: 2. Lessons learned from recent passive remediation experiences. Environ. Sci. Pollut. Res. 20 (11), 7837–7853.

Balci, N., Shanks III, W.C., Mayer, B., Mandernack, K.W., 2007. Oxygen and sulfur isotopic systematics of sulfate produced during bacterial and abiotic oxidation of pyrite. Geochim. Cosmochim. Acta 71, 3796–3811.

Balci, N., Mayer, B., Shanks III, W.C., Mandernack, K.W., 2012. Oxygen and sulfur isotope systematics of sulfate produced during abiotic and bacterial oxidation of sphalerite and elemental sulfur. Geochim. Cosmochim. Acta 77, 335–351.

Balci, N., Brunner, B., Turchyn, A.V., 2017. Tetrathionate and elemental sulfur shape the isotope composition of sulfate in acid mine drainage. Front. Microbiol. 8, 1564.

Bao, H., Jenkins, K.A., Khachaturyan, A., Chong, G., 2004. Different sulfate sources and their post-depositional migration in Atacama soils. Earth Planet. Sci. Lett. 224, 577–587.

Bao, R., Hernández, A., Sáez, A., Giralt, S., Prego, R., Pueyo, J.J., Moreno, A., Valero-Garcés, B.L., 2015. Climatic and lacustrine morphometric controls of diatom paleoproductivity in a tropical Andean lake. Quat. Sci. Rev. 129, 96–110.

Barton, M.D., Johnson, D.A., 1996. Evaporitic-source model for igneous related Fe oxide-(REE-Cu-Au-U) mineralization. Geology 24 (3), 259–262.

Benison, K.C., 2006. A Martian analog in Kansas: comparing Martian strata with Permian acid saline lake deposits. Geology 34 (5), 385–388.

Benison, K.C., 2019. The physical and chemical sedimentology of two high-altitude acid salars in Chile: sedimentary processes in an extreme environment. J. Sediment. Res. 89, 147–167.

Benison, K.C., Bowen, B.B., 2006. Acid saline lake systems give clues about past environments and the search for life on Mars. Icarus 183, 225–229.

Benison, K.C., Bowen, B.B., 2013. Extreme sulfur-cycling in acid brine lake environments of Western Australia. Chem. Geol. 351, 154–167.

Benison, K.C., Bowen, B.B., 2015. The evolution of end-member continental waters: the origin of acidity in southern Western Australia. GSA Today 25 (6), 4–10.

Benison, K.C., Goldstein, R.H., 2002. Recognizing acid lakes and groundwaters in the rock record. Sediment. Geol. 151, 177–185.

Benison, K.C., Karmanocky III, F.J., 2014. Could microorganisms be preserved in Mars gypsum? Insights from terrestrial examples. Geology 42 (7), 615–618.

Benison, K.C., Goldstein, R.H., Wopenka, B., Burruss, R.C., Pasteris, J.D., 1998. Extremely acid Permian lakes and ground waters in North America. Nature 392, 911–914.

Benison, K.C., Bowen, B.B., Oboh-Ikuenobe, F.E., Jagniecki, E.A., LaClair, D.A., Story, S. L., Mormile, M.R., Hong, B., 2007. Sedimentology of acid lakes in southern western Australia: newly described processes and products of an extreme environment. J. Sediment. Res. 77, 366–388.

Bethke, P.M., Rye, R.O., Stoffregen, R.E., Vikre, P.G., 2005. Evolution of the magmatic-hydrothermal acid-sulfate system at Summitville, Colorado: integration of geological, stable isotope and fluid-inclusion evidence. Chem. Geol. 215, 281–315.

Betts, R.H., Voss, R.H., 1970. The kinetics of oxygen exchange between the sulfite ion and water. Can. J. Chem. 48, 2035–2041.

Bibring, J.P., Langevin, Y., Mustard, J.F., Poulet, F., Arvidson, R., Gendrin, A., Gondet, B., Mangold, N., Pinet, P., Forget, F., the Omega Team, 2006. Global mineralogical and aqueous Mars history derived from Omega/Mars Express data. Science 312, 400–404.

Bird, M.I., Andrew, A.S., Chivas, A.R., Lock, D.E., 1989. An isotopic study of surficial alunite in Australia 1: hydrogen and sulfur isotopes. Geochim. Cosmochim. Acta 53, 3223–3237.

Bissig, T., Riquelme, R., 2010. Andean uplift and climate evolution in the southern Atacama Desert deduced from geomorphology and supergene alunite-group minerals. Earth Planet. Sci. Lett. 299, 447–457.

Blatt, H., Middleton, G., Murray, R., 1972. Origin of Sedimentary Rocks. Prentice-Hall (330p).

Böhlke, J.K., Ericksen, G.E., Revesz, K., 1997. Stable isotope evidence for an atmospheric origin of desert nitrate deposits in northern Chile and southern California, USA. Chem. Geol. 136, 135–152.
Bond, P.L., Druschel, G.K., Banfield, J.F., 2000a. Comparison of acid mine drainage microbial communities in physically and geochemically distinct ecosystems. Appl. Environ. Microbiol. 66 (11), 4962–4971.
Bond, P.L., Smriga, S.P., Banfield, J.F., 2000b. Phylogeny of microorganisms populating a thick, subaerial, predominantly lithotrophic biofilm at an extreme acid mine drainage site. Appl. Environ. Microbiol. 66 (9), 3842–3849.
Brabec, M.Y., Lyons, T.W., Mandernack, K.W., 2012. Oxygen and sulfur isotope fractionation during sulfide oxidation by anoxygenic phototrophic bacteria. Geochim. Cosmochim. Acta 83, 234–251.
Brennan, B.J., 2003. Beta doses to spherical grains. Radiat. Meas. 37, 299–303.
Brunner, B., Yu, J.Y., Mielke, R.E., MacAskill, Madzunkov, S., Mc Genity, T.J., Coleman, M., 2008. Different isotope and chemical patterns of pyrite oxidation related to lag and exponential growth phases of *Acidithiobacillus ferrooxidans* reveal a microbial growth strategy. Earth Planet. Sci. Lett. 270, 63–72.
Brunner, B., Einsiedl, F., Arnold, G.L., Muller, I., Templer, S., Bernasconi, S.M., 2012. The reversibility of dissimilatory sulphate reduction and the cell-internal multi-step reduction of sulphite to sulphide: insights from the oxygen isotope composition of sulphate. Isot. Environ. Health Stud. 48 (1), 33–54.
Carmona, V., 2002. *Gènesi i Funcionament Hidroquímic del Salar d'Atacama (N. de Xile).* Tesi Doctoral. Facultat de Geologia. Universitat de Barcelona (138p).
Carmona, V., Pueyo, J.J., Taberner, C., Chong, G., Thirlwall, M., 2000. Solute inputs in the Salar de Atacama (N Chile). J. Geochem. Explor. 69–70, 449–452.
Cendón, D.I., Peryt, T., Ayora, C., Pueyo, J.J., Taberner, C., 2004. The importance of recycling processes in the Middle Miocene Badenian evaporite basin (Carpathian foredeep): palaeoenvironmental implications. Palaeogeogr. Palaeoclimatol. Palaeoecol. 212, 141–158.
Chaffaut, I., Coudrain, A., Michelot, J.L., Pouyaud, B., 1998. Précipitations d'altitude du Nord-Chili, origine des sources de vapeur et données isotopiques. Bull. Inst. fr. Études Andines 27 (3), 367–384.
Chiba, H., Sakai, H., 1985. Oxygen isotope exchange rate between dissolved sulfate and water at hydrothermal temperatures. Geochim. Cosmochim. Acta 49 (4), 993–1000.
Chivas, A.R., Andrew, A.S., Lyons, W.B., Bird, M.I., Donnelly, T.H., 1998. Isotopic constraints on the origin of salts in Australian playas. 1. Sulfur. Palaeogeogr. Palaeoclimatol. Palaeoecol. 84 (1–4), 309–332.
Chong, G., 1984. Die Salare in Nordchile: geologie, struktur und geochemie. Schweizerbart'sche Verlagsbuchhandlung, Stutgart (146 pp).
Chong, G., Demergasso, C., Urrutia-Meza, J., Vargas, M., 2020. El Dominio Salino del norte de Chile y sus yacimientos de minerales industriales. Boletín de la Sociedad Geológica Mexicana 72 (3), A020720. https://doi.org/10.18268/BSGM2020v72n3a020720.
Chong, G., Mendoza, M., García-Veigas, J., Pueyo, J.J., Turner, P., 1999. The Salar Grande (Central Andes of Chile). Evolution and environmental records in a Neogene evaporitic basin. Palaeogeogr. Palaeoclimatol. Palaeoecol. 151 (1–4), 39–54.
Chong, G., 1994. The nitrate deposits of Chile. In: Reutter, K.J., Scheuber, E., Wigger, P.J. (Eds.), Tectonic of the Southern Central Andes. Structure and Evolution of an active continental margin. Springer, pp. 303–316.
Chong, G., Cortés, P., Escudero, P., Bijman, J., Pueyo, J.J., Demergasso, C., 2015. Geomicrobiology in an acid hypersaline system in Northern Chile. In: *XIV Congreso Geológico Chileno*, La Serena, 4–8 October 2015. Abstracts, pp. 725–728.
Claypool, G.E., Holser, W.T., Kaplan, I.R., Sakai, H., Zak, I., 1980. The age curves of sulfur and oxygen isotopes in marine sulfate and their interpretation. Chem. Geol. 28, 199–260.
Coleman, M.J., 1977. Sulphur isotopes in petrology. J. Geol. Soc. 133, 593–608.
Cornejo, P., 1987. Hydrothermal alteration zones and sulphur deposits in upper Cenozoic volcanoes of Salar de Gorbea, Andes of northern Chile. Pac. Rim Congress 87, 877–885.
Cortéz, P.A., 2014. Caracterización Geológica de los Salares Gorbea e Ignorado y su Asociación con su Microbiota. Memoria para optar al título de geólogo. Universidad Católica del Norte, Antofagasta (222 p).
Davila, A.F., Fairén, A.G., Gago-Duport, L., Stoker, C., Amils, R., Bonaccorsi, R., Zavaleta, J., Lim, D., Schulze-Makuch, D., McKay, Ch.P., 2008. Subsurface formation of oxidants on Mars and implications for the preservation for organic biosignatures. Earth Planet. Sci. Lett. 272, 456–463.
Davis-Belmar, C.S., Pinto, E., Demergasso, C.S., Rautenbach, G., 2013. Proteo and Actinobacteria diversity at a sulfide, salt and acid-rich lake in the North of Chile. Adv. Mater. Res. 825, 37–41.
de Silva, S.L., 1989. Altiplano-Puna volcanic complex of the Central Andes. Geology 17, 1102–1106.
Demergasso, C., Casamayor, E.O., Chong, G., Galleguillos, P., Escudero, L., Pedros-Alió, C., 2004. Distribution of prokaryotic genetic diversity in athalassohaline lakes of the Atacama Desert, Northern Chile. FEMS Microbiol. Ecol. 48 (1), 57–69.
Demergasso, C., Escudero, L., Casamayor, E.O., Chong, G., Balague, V., Pedros-Alió, C., 2008. Novelty and spatio-temporal heterogeneity in the bacterial diversity of hypersaline Lake Tebenquiche (Salar de Atacama). Extremophiles 12 (4), 491–504.
Demergasso, C., Pueyo, J.J., Escudero, L., Chong, G., Cortéz, P., Bijman, J., 2014. Is arsenic available as energy source for microbial growth in acidic and hypersaline lakes?. In: *Goldschmidt Conference,* Sacramento 8-13th June 2014. Abstracts 528.
Deyell, C.L., Rye, R.O., Landis, G.P., Bissig, T., 2005. Alunite and the role of magmatic fluids in the Tambo high-supfidation deposit, El Indio-Pascua belt, Chile. Chem. Geol. 215, 185–218.
Diaby, N., Dold, B., Pfeifer, H.R., Holliger, C., Johnson, D.B., Hallberg, K.B., 2007. Microbial communities in a porphyry copper tailings impoundment and their impact on the geochemical dynamics of the mine waste. Environ. Microbiol. 9 (2), 298–307.
Dickson, B.L., Giblin, A.M., 2009. Features of acid-saline systems of Southern Australia. Appl. Geochem. 24, 297–302.
Dold, B., Fontboté, L., 2001. Element cycling and secondary mineralogy in porphyry copper tailings as a function of climate, primary mineralogy, and mineral processing. J. Geochem. Explor. 74 (1–3), 3–55.
Dold, B., Fontboté, L., 2002. A mineralogical and geochemical study of element mobility in sulfide mine tailings of Fe oxide Cu-Au deposits from the Punta del Cobre belt, northern Chile. Chem. Geol. 189 (3–4), 135–163.
Dold, B., Spangenberg, J.E., 2005. Sulfur speciation and stable isotope trends of water-soluble sulfates in mine tailings profiles. Environ. Sci. Technol. 39 (15), 5650–5656.
Egal, M., Elbaz-Poulichet, F., Casiot, C., Motelica-Heino, M., Négrel, P., Bruneel, O., Sarmiento, A.M., Nieto, J.M., 2008. Iron isotopes in acid saline waters and iron rich solids from the Tinto-Odiel Basin (Iberian Pyrite Belt, Southwest Spain). Chem. Geol. 253, 162–171.
El Tabakh, M., Riccioni, R., Schreiber, B.C., 1997. Evolution of late Triassic rift basin evaporites (Passaic Fm): Newark basin, eastern N America. Sedimentology 44 (4), 767–790.
Engel, Z., Skrzypek, G., Chuman, T., Sefrna, L., Mihaljevic, M., 2014. Climate in the Western Cordillera of the Central Andes over the last 4300 years. Quat. Sci. Rev. 99, 60–77.
Ericksen, G.E., 1981. Geology and Origin of Chilean Nitrate Deposits. *US Geological Survey Professional Paper* 1188 (37pp).
Escudero, L.W., Bijman, J., Chong, G., Pueyo, J.J., Demergasso, C., 2013. Geochemistry and microbiology in an acidic high altitude (4000m) salt flat, high Andes, Northern Chile. Adv. Mater. Res. 825, 28–32.
Escudero, L.W., Oetiker, N., Gallardo, K., Tebes-Cayo, C., Guajardo, M., Núñez, C., Davis-Belmar, C., Pueyo, J.J., Chong, G., Demergasso, C., 2018. A thiotrophic microbial comunity in an acidic brine lake in Northern Chile. Antonie Van Leeuwenhoek 111 (8), 1403–1419.
Fernández-Remolar, D.C., Morris, R.V., Gruener, J.E., Amils, R., Knoll, A.H., 2005. The Rio Tinto Basin, Spain: Mineralogy, sedimentary geobiology, and implications for the interpretation of outcrop rocks at Meridiani Planum, Mars. Earth Planet. Sci. Lett. 240, 149–167.
Froger, J.L., Remy, D., Bonvalot, S., Legrand, D., 2007. Two scales of inflation at Lastarria – Cordon del azufre complex, Central Andes, revealed from ASAR-ENVISAT interferometric data. Earth Planet. Sci. Lett. 255, 148–163.
Frost, R.L., Weier, M., Martínez-Frías, J., Rull, F., Reddy, J., 2007. Sulphate efflorescent minerals from El Jaroso Ravine, Sierra Almagrera – a SEM and Raman spectroscopic study. Spectrochim. Acta A 66, 177–183.
Fry, B., Cox, Gest, H., Hayes, J.M., 1986. Discrimination between ^{34}S and ^{32}S during bacterial metabolism of inorganic sulfur compounds. J. Bacteriol. 165, 328–330.
García, M., Riquelme, R., Farías, M., Hérail, G., Charrier, R., 2011. Late Miocene–Holocene canyon incision in the western Altiplano, northern Chile: tectonic or climatic forcing? J. Geol. Soc. Lond. 168, 1047–1060.
Gázquez, F., Evans, N.P., Hodell, D.A., 2017. Precise and accurate isotope fractionation factors (α17O, α18O ans αD) for water and CaSO4·2H2O (gypsum). Geochim. Cosmochim. Acta 198, 259–270.
García-Moyano, A., González-Toril, E., Aguilera, A., Amils, R., 2012. Comparative microbial ecology study of the sediments and the water column of the Rio Tinto, an extreme acidic environment. FEMS Microbiol. Ecol. 81 (2), 303–314.
Geng, M., Duan, Z., 2010. Prediction of oxygen solubility in pure water and brines up to high temperatures and pressures. Geochim. Cosmochim. Acta 74 (19), 5631–5640.
Gibert, R.O., Taberner, C., Sáez, A., Giralt, S., Alonso, R.N., Edwards, R.L., Pueyo, J.J., 2009. Igneous origin of CO_2 in ancient and recent hot-spring waters and travertines from the northern Argentinean Andes. J. Sediment. Res. 79, 554–567.
Giralt, S., Moreno, A., Bao, R., Sáez, A., Prego, R., Valero-Garcés, B.L., Pueyo, J.J., González-Sampériz, P., Taberner, C., 2008. A statistical approach to disentangle environmental forcings in a lacustrine record: the Lago Chungará case (Chilean Altiplano). J. Paleolimnol. 40, 195–215.
Godfrey, L., Alvarez-Amado, F., 2020. Volcanic and saline lithium inputs to the Salar de Atacama. Minerals 10 (2), 201. https://doi.org/10.3390/min10020201.
González-Toril, E., Llobet-Brossa, E., Casamayor, E.O., Amann, R., Amils, R., 2003. Microbial ecology of an extreme acidic environment, the Tinto river. Appl. Environ. Microbiol. 69 (11), 4853–4865.
González-Toril, E., Santofimia, E., Blanco, Y., López-Pamo, E., Gómez, M.J., Bobadilla, M., Cruz, R., Palomino, E.J., Aguilera, A., 2015. Pyrosequencing-based Assessment of the Microbial Community Structure of Pastoruri Glacier Area (Huascaran National Park, Peru), a Natural Extreme Acidic Environment. Microb. Ecol. 70 (4), 936–947.
Gosh, W., Dam, B., 2009. Biochemistry and molecular biology of lithotrophic sulfur oxidation by taxonomically and ecologically diverse bacteria and archaea. FEMS Microbiol. Rev. 33 (6), 999–1043.
Grosjean, M., Santoro, C.M., Thomson, L.G., Núñez, L., Standen, V.G., 2007. In: Anderson, D.G., Maasch, K.A., Sandweiss, H.H. (Eds.), Climate change and cultural dynamics: A global perspective on Mid-Holocene transitions. Elsevier Eds. Chap: 3.
Guerin, G., Mercier, N., Adamiec, G., 2011. Dose-rate conversion factors: update. Ancient TL 29, 5–8.
Hammarstrom, J.M., Seal II, R.R., Meier, A.L., Kornfeld, J.M., 2005. Secondary sulfate minerals associated with acid drainage in the eastern US: recycling of metals and acidity in surficial environments. Chem. Geol. 215, 407–431.
Hastenrath, S.L., 1971. On the Pleistocene snow-line depression in the arid regions of the South American Andes. J. Glaciol. 10 (59), 255–267.
Hedenquist, J.W., Simmons, S.F., Giggenbach, W.F., Eldridge, C.S., 1993. White Island, New Zealand, volcanic hydrothermal system represents the geochemical environment of high sulfidation Cu and Au ore de-position. Geology 21, 731–734.

Herrera, C., Pueyo, J.J., Sáez, A., Valero-Garcés, B.L., 2006. Relación de aguas superficiales y subterráneas en el área del lago Chungará y lagunas de Cotacotani, norte de Chile: un estudio isotópico. Rev. Geol. Chile 33 (2), 299–325.
Hoke, G.D., Isacks, B.L., Jordan, T.E., Yu, J.S., 2004. Groundwater-sapping origin for the giant quebradas of northern Chile. Geology 32 (7), 605–608.
Hoke, G.D., Isacks, B.L., Jordan, T.E., Blanco, N., Tomlinson, A.J., Ramezani, J., 2007. Geomorphic evidence for post-10 Ma uplift of the western flank of the Central Andes 18° 30′ - 22° S. Tectonics 26, TS5021.
Hopper, D., Correa, A., 2000. The Panulcillo and Teresa de Colmo copper deposits: two contrasting examples of Fe-ox Cu-Au mineralisation from the Coastal Cordillera of Chile. In: Porter, T.M. (Ed.), Hydrothermal Iron Oxide Copper-Gold & Related Deposits. A Global Perspective, 1. PGC Publishing, Adelaide, pp. 177–189.
Hubbard, C.G., Black, S., Coleman, M.L., 2009. Aqueous geochemistry and oxygen isotopic compositions of acid mine drainage from the Rio Tinto, SW Spain, highlight inconsistencies in current models. Chem. Geol. 265, 321–334.
Igarzábal, A., 1979. Los rasgos Geomorfológicos y su Relación con el origen del Salar de Pastos Grandes, Departamento de Los Andes, Provincial de Salta. Actas del VII Congreso Geológico Argentino, I, pp. 199–209.
Igarzábal, A., 1991. Evaporitas cuaternarias de la Puna argentina. In: Pueyo, J.J. (Ed.), Génesis de Formaciones Evaporíticas. Modelos Andinos e Ibéricos. Estudi General Publicacions Universitat de Barcelona, pp. 333–374.
John, D.A., Sisson, T.H., Breit, G.N., Rye, R.O., Wallance, J.W., 2008. Characteristics, extent and origin of hydrothermal alteration at Mount Rainier Volcano, Cascades Arc, USA: implications for debris-flow hazards and mineral deposits. J. Volcanol. Geotherm. Res. 175, 289–314.
Johnson, S.S., Chevrette, M.G., Ehlmann, B.L., Benison, K.C., 2015. Insights from the metagenome of an acid salt lake: the role of biology in an extreme depositional environment. PLoS One 10 (4), e0122869.
Karmanocky, F.J., Benison, K.C., 2016. A fluid inclusion record of magmatic hydrothermal pulses in acid Salar Ignorado gypsum, northern Chile. Geofluids 16, 490–506.
Korehi, H., Blothe, M., Sitnikova, M.A., Dold, B., Schippers, A., 2013. Metal Mobilization by Iron- and Sulfur-Oxidizing Bacteria in a Multiple Extreme Mine Tailings in the Atacama Desert, Chile. Environ. Sci. Technol. 47 (5), 2189–2196.
Leybourne, M.I., Cameron, E.M., 2006. Composition of groundwater associated with porphyry-Cu deposits, Atacama Desert, Chile: Elemental and isotopic constraints on water sources and water-rock reactions. Geochim. Cosmochim. Acta 70, 1616–1635.
Leybourne, M., Cameron, E.M., Reich, M., Palacios, C., Faure, K., Johannesson, K.H., 2013. Stable isotopic composition of soil calcite (O, C) and gypsum (S) overlying Cu deposits in the Atacama Desert, Chile: Implications for mineral exploration, salt sources, and paleoenvironmental reconstruction. Appl. Geochem. 29, 55–72.
Lloyd, R.M., 1967. Oxygen-18 composition of oceanic sulfate. Science 156, 1228–1231.
Lloyd, R.M., 1968. Oxygen isotope behavior in the sulfate-water system. J. Geophys. Res. 73, 6099–6110.
Long, D.T., Lyons, W.B., 1992. Aridity, continental weathering and ground water chemistry. GSA Today 2 (9), 185–190.
Long, D.T., Fegan, N.E., McGee, J.D., Lyons, W.B., Hines, M.E., Macumber, P.G., 1992. Formation of alunite, jarosite and hydrous oxides in a hypersaline system: Lake Tyrrell, Victoria, Australia. In: Lyons, W.B., Long, D.T., Herczeg, A.L., Hines, M.E. (Eds.), The Geochemistry of Acid Groundwater Systems, 96. Chemical Geology, pp. 183–202.
Lurgo Mayón, C., 1999. Azufre volcanogénico de la Puna, Jujuy, Salta y Catamarca. In: Zappettini, E. (Ed.), Recursos Minerales de la República Argentina. Buenos Aires, Argentina. SEGEMAR. Anales 35: 1613-1625.
Lybrand, R.A., Bockheim, J.G., Ge, W., Graham, R., Hlohowskyj, S.R., 2016. Nitrate, perchlorate and iodate co-occur in coastal and inland deserts on Earth. Chem. Geol. 442, 174–186.
Macumber, P.G., 1992. Hydrological processes in the Tyrrell Basin, southeastern Australia. Chem. Geol. 96, 1–18.
Magaritz, M., Aravena, R., Peña, H., Suzuki, O., Grilli, A., 1989. Water chemistry and isotope study of streams and springs in northern Chile. J. Hydrol. 108, 323–341.
Mandakovic, D., Maldonado, J., Pulgar, R., Cabrera, P., Gaete, A., Urtuvia, V., Seeger, M., Cambiazo, V., González, M., 2018. Microbiome analysis and bacterial isolation from Lejia Lake soil in Atacama Desert. Extremophiles 22 (4), 665–673.
Marion, G.M., Crowley, J.K., Thompson, B.J., Kargel, J.S., Bridges, N.T., Hook, S.J., Baldridge, A., Brown, A.J., Ribeiro da Luz, B., de Souza-Filho, C.R., 2009. Modelling aluminium-silicon chemistries and application to Australian acidic playa lakes as analogues for Mars. Geochim. Cosmochim. Acta 73, 3493–3511.
McArthur, J.M., Turner, J.V., Lyons, W.B., Osborn, A.O., Thirlwall, M.F., 1991. Hydrochemistry of the Yilgarn Block, Western Australia: ferrolysis and mineralization in acidic brines. Geochim. Cosmochim. Acta 55 (5), 1273–1288.
Michalski, G., Böhlke, J.K., Thiemens, M., 2004. Long term atmospheric deposition as the source of nitrate and other salts in the Atacama Desert, Chile: New evidence from mass-independent oxygen isotopic compositions. Geochim. Cosmochim. Acta 68 (20), 4023–4038.
Momenzadeh, M., 1990. Saline deposits and alkaline magmatism: a genetic model. J. Pet. Geol. 13, 341–356.
Mormile, M.R., Hong, B.-Y., Benison, K.C., 2009. Molecular Analysis of the Microbial Communities of Mars Analog Lakes in Western Australia. Astrobiology 9 (10), 919–930.
Müller, I.A., Brunner, B., Breuer, C., Coleman, M., Bach, W., 2013a. The oxygen isotope equilibrium fractionation between sulfite species and water. Geochim. Cosmochim. Acta 120, 562–581.
Müller, I.A., Brunner, B., Coleman, M., 2013b. Isotopic evidence of the pivotal role of sulfite oxidation in shaping the oxygen isotopic signature of sulfate. Chem. Geol. 354, 186–202.
Murray, A.S., Wintle, A.G., 2000. Luminescence dating of quartz using an improved single-aliquot regenerative-dose protocol. Radiat. Meas. 32, 57–73.
Murray, A.S., Wintle, A.G., 2003. The single aliquot regenerative dose protocol: potential for improvements in reliability. Radiat. Meas. 37, 377–381.
Naranjo, J.A., 1985. Sulphur flows at Lastarria volcano in the North Chilean Andes. Nature 313, 778–780.
Naranjo, J.A., 1986. Geology and Evolution of the Lastarria Volcanic Complex, North Chilean Andes. M.Phil. Thesis. Open University, England.
Naranjo, J.A., 1988. Coladas de azufre de los volcanes Lastarria y Bayo en el norte de Chile: reología, génesis e importancia planetaria. Rev. Geol. Chile 31, 43–55.
Naranjo, J.A., Puig, A., 1984. *Geología de Las Hojas de Taltal y Chañaral.* Carta Geológica de Chile. SERNAGEOMIN, pp. 62–63 (140 pp).
Newman, D.K., Banfield, J.F., 2002. Geomicrobiology: how molecular-scale interactions underpin biogeochemical Systems. Science 296, 1071–1077.
Ohlanders, N., Rodríguez, M., McPhee, J., 2013. Stable water isotope variation in a Central Andean watershed dominated by glacier and snowmelt. Hydrol. Earth. Syst. Sci. 17, 1035–1050.
Ortí, F., Pueyo, J.J., Geisler-Cussey, D., Dulau, N., 1984. Evaporitic sedimentation in the coastal Salinas of Santa Pola (Alicante, Spain). Rev. Inv. Geol. 38/39, 169–220.
Paduano, G.M., Bush, M.B., Baker, P.A., Fritz, S.C., Seltzer, G.O., 2003. A vegetation and fire history of Lake Titicaca since the last Glacial Maximum. Palaeogeogr. Palaeoclimatol. Palaeoecol. 194, 259–279.
Parra, A., Oyarzun, J., Maturana, H., Kretschmer, N., Meza, F., Oyarzun, R., 2011. Natural factors and mining activity bearings on the water quality of the Choapa basin, North Central Chile: insights on the role of mafic volcanic rocks in the buffering of the acid drainage process. Environ. Monit. Assess. 181 (1–4), 69–82.
Placzek, Ch., Quade, J., Patchett, P.J., 2006. Geochronology and stratigraphy of the late Pleistocene lake cycles on the southern Bolivian Altiplano: implications for causes of tropical climate change. GSA Bull. 118 (5/6), 515–532.
Pellerin, A., Antler, G., Holm, S.A., Findlay, A.J., Crockford, P.W., Turchyn, A.V., Jorgensen, B.B., Finster, K., 2019. Large sulfur isotope fractionation by bacterial sulfide oxidation. Science Advances 5 (7), eeaw1480. https://doi.org/10.1126/sciadv.aaw1480.
Placzek, Ch., Matmon, A., Granger, D.E., Quade, J., Niedermann, S., 2010. Evidence for active landscape evolution in the hyperarid Atacama from multiple terrestrial cosmogenic nuclides. Earth Planet. Sci. Lett. 295, 12–20.
Prescott, R.R., Hutton, J.T., 1994. Cosmic ray contributions to dose rates for luminescence and ESR dating: large depths and long term time variations. Radiat. Meas. 23, 497–500.
Pueyo, J.J., Chong, G., Jensen, A., 2001. Neogene evaporites in desert volcanic environments: Atacama Desert, northern Chile. Sedimentology 48 (6), 1411–1431.
Pueyo, J.J., Sáez, A., Giralt, S., Valero-Garcés, B.L., Moreno, A., Bao, R., Schwalb, A., Herrera, Ch., Klosowska, B., Taberner, C., 2011. Carbonate and organic matter sedimentation and isotopic signatures in Lake Chungará, Chilean altiplano, during the last 12.3 kyr. Palaeogeogr. Palaeoclimatol. Palaeoecol. 307, 339–355.
Qin, Y., Li, Y., Bao, H., Liu, F., Hou, K., Wan, D., Zhang, C., 2012. Massive atmospheric nitrate accumulation in a continental interior desert, northwestern China. Geology 40 (7), 623–626.
Quade, J., Rech, J.A., Betancourt, J.L., Latorre, C., Quade, B., Rylander, K.A., Fisher, T., 2008. Paleowetlands and regional climate change in the Central Atacama Desert, northern Chile. Quat. Res. 69, 343–360.
Quatrini, R., Escudero, L., Moya-Beltrán, A., Galleguillos, P.A., Issotta, F., Acosta, M., Cárdenas, J.P., Núñez, H., Salinas, K., Holmes, D., Demergasso, C., 2017. Draft genome sequence of Acidithiobacillus thiooxidans CLST isolated from the acídic hypersaline Gorbea salt flat in Northern Chile. Stand. Genomic Sci. 12, 84. https://doi.org/10.1186/s40793-017-0305-8.
Ramirez, C.F., Gardeweg, M., 1982. *Hoja Toconao, Región de Antofagasta*. Serv. Nac. Geol. Min., Carta Geol. Chile n° 54.
Rech, J.A., Quade, J., Hart, W.S., 2003. Isotopic evidence for the source of Ca and S in soil gypsum, anhydrite and calcite in the Atacama Desert, Chile. Geochim. Cosmochim. Acta 67 (4), 575–586.
Rech, J.A., Currie, B.S., Michalski, G., Cowan, A.M., 2006. Neogene climate change and uplift in the Atacama Desert, Chile. Geol. Soc. Am. 34 (9), 761–764.
Rech, J.A., Currie, B.S., Shullenberger, E.D., Dunagan, S.P., Jordan, T.E., Blanco, N., Tomlinson, A.J., Rowe, H.D., Houston, J., 2010. Evidence for the development of the Andean rain shadow from a Neogene isotopic record in the Atacama Desert, Chile. Earth Planet. Sci. Lett. 292, 371–382.
Rech, J.A., Currie, B.S., Jordan, T.E., Riquelme, R., Lehmann, S.B., Kirk-Lawlor, N.E., Li, S., Gooley, J.T., 2019. Massive middle Miocene gypsic paleosols in the Atacama Desert and the formation of the Central rain-shadow. Earth Planet. Sci. Lett. 506, 184–194.
Reich, M., Bao, H., 2018. Nitrate deposits of the Atacama Desert: a marker of Long-Term Hyperaridity. Elements 14, 251–256.
Reich, M., Palacios, C., Vargas, G., Luo, S., Cameron, E.M., Leybourne, M.I., Parada, M. A., Zúñiga, A., You, Ch.F., 2009. Supergene enrichment of copper deposits since the onset of modern hyperaridity in the Atacama Desert, Chile. Mineral. Deposita 44, 497–504.
Richards, J.P., Villeneuve, M., 2002. Characteristics of late Cenozoic volcanism along the Archibarca lineament from Cerro Llullaillaco to Corrida de Cori, Northwest Argentina. J. Volcanol. Geotherm. Res. 116, 161–200.
Risacher, F., Fritz, B., 2000. Bromine geochemistry of Salar de Uyuni and deeper salt crusts, Central Altiplano, Bolivia. Chem. Geol. 3-4, 373–392.
Risacher, F., Alonso, H., Salazar, C., 1999. *Geoquímica de Aguas en Cuencas Cerradas: I, II y III Regiones – Chile. Vol. IV: Estudio de Cuencas de la III region.* S.I.T. n° 51 (247 pp).
Risacher, F., Alonso, H., Salazar, C., 2002. Hydrochemistry of two adjacent acid saline lakes in the Andes of northern Chile. Chem. Geol. 187, 39–57.

Risacher, F., Alonso, H., Salazar, C., 2003. The origin of brines and salts in Chilean salars: a hydrochemical review. Earth Sci. Rev. 63, 249–293.
Risacher, F., Fritz, B., Hauser, A., 2011. Origin of components in Chilean thermal waters. J. S. Am. Earth Sci. 31, 153–170.
Rissmann, C., Leybourne, M., Benn, C., Christenson, B., 2015. The origin of solutes within the groundwaters of a high Andean aquifer. Chem. Geol. 396, 164–181.
Rohrssen, M., Brunner, B., Mielke, R.E., Coleman, M., 2008. Method for simultaneous oxygen and hydrogen isotope analysis of water of crystallization in hydrated minerals. Anal. Chem. 80, 7084–7089.
Romero, A., González, I., Galán, E., 2006. The role of efflorescent sulphates in the storage of trace elements in stream waters polluted by acid mine-drainage: the case of Peña del Hierro, Southwestern Spain. Can. Mineral. 44, 1431–1446.
Ruch, J., Walter, T.R., 2010. Relationship between the InSAR-measured uplift, the structural framework, and the present-day stress field at Lazufre volcanic area, Central Andes. Tectonophysics. 492 (1–4), 133–140.
Rye, R.O., 2005. A review of the stable-isotope geochemistry of sulfate minerals in selected igneous environments and related hydrothermal systems. Chem. Geol. 215, 5–36.
Rye, R.O., Alpers, C.N., 1997. The stable isotope geochemistry of jarosite. In: US Geological Survey. Open-File Report (97–88, 28pp).
Rye, R.O., Bethke, P.M., Wasserman, M.D., 1989. Diverse origins of alunite and acid-sulfate alteration: stable isotope systematics. In: US Geological Survey. Open-File Report, 89-5, pp. 1–33.
Rye, R.O., Bethke, P.M., Wasserman, M.D., 1992. The stable isotope geochemistry of acid sulfate alteration. Econ. Geol. 87, 225–262.
Rye, R.O., Bethke, P.M., Lanphere, M.A., Steven, T.A., 2000. Neogene Geomorphic and Climate Evolution of the Central San Juan Mountains, Colorado: K/Ar Age and Stable Isotope Data on Supergene Alunite and Jarosite from the Creede Mining District. GSA Special Papers, 346, pp. 95–103.
Sáez, A., Valero-Garcés, B.L., Moreno, A., Bao, R., Pueyo, J.J., González-Sampériz, P., Giralt, S., Taberner, C., Herrera, C., Gibert, R.O., 2007. Volcanic controls on lacustrine sedimentation: the late Quaternary depositional evolution of lake Chungará (northern Chile). Sedimentology 54, 1191–1222.
Sáez, A., Cabrera, L., Garcés, M., van der Bogaard, P., Jensen, A., Gimeno, D., 2012. The stratigraphic record of changing hyperaridity in the Atacama Desert over the last 10 Ma. Earth Planet. Sci. Lett. 355-356, 32–38 (32–28).
Sáez, A., Godfrey, L., Herrera, Ch., Chong, G., Pueyo, J.J., 2016. Timing of wet episodes in Atacama Desert over the last 15 ka. The Groundwater Discharge Deposits (GWD) from Domeyko Range at 25°S. Quat. Sci. Rev. 145, 82–93.
Scheuber, E., Bogdanic, T., Jensen, A., Reutter, K.J., 1994. Tectonic development of the North Chilean Andes in relation to plate convergence and magmatism since the Jurassic. In: *Tectonics of the Southern Central Andes* (K.J. Reutter et al., eds). Springer, Berlin, pp. 121–139.
Schimmelmann, A., 2014. Hydrogen, Carbon, Nitrogen and Oxygen Stable Isotope Reference Materials from Indiana University. http://mypage.iu.edu/~aschimme/files/alphabetical%20list%20of%20all%20reference%20materials.pdf.
Seal II, R.R., 2006. Sulfur isotope geochemistry of sulfide minerals. Rev. Mineral. Geochem. 61, 633–677.
Seal II, R.R., Alpers, C.N., Rye, R.O., 2000. Stable isotope systematics of sulfate minerals. In: Alpers, C.N., Jambor, J.L., Nordstrom, D.K. (Eds.), *Sulfate Minerals: Crystallography, Geochemistry, and Environmental Significance.* Mineralogical Society of America and Geochemical Society, 40. Reviews in Mineralogy and Geochemistry, Washington, D.C, pp. 541–602.
Sillitoe, R.H., 1993. Epithermal models: Genetic types, geometrical controls and shallow features. In: Kirkham, R.V., Sinclair, W.D., Thorpe, R.I., Duke, J.M. (Eds.), Mineral Deposit Modeling, 40. Geological Association of Canada, pp. 403–417. Special Paper.
Sillitoe, R.H., 1999. Styles of High-Sulphidation Gold, Silver and Copper Mineralisation in Porphyry and Epitermal Environments. *PACRIM'99.* Bali, Indonesia 10-13 October 1999, pp. 29–44.
Simmons, S.F., White, N.C., John, D.A., 2005. Geological characteristics of epithermal precious and base metal deposits. Econ. Geol. 100, 485–522.
Singer, P.C., Stumm, W., 1970. Acid mine drainage: the rate-determining step. Science 167, 1121–1123.
Smuda, J., Dold, B., Spangenberg, J.E., Friese, K., Kobek, M.R., Bustos, C.A., Pfeifer, H.R., 2014. Element cycling during the transition from alkaline to acidic environment in an active porphyry copper tailings impoundment, Chuquicamata, Chile. J. Geochem. Explor. 140, 23–40.
Spangenberg, J.E., Dold, B., Vogt, M.L., Pfeifer, H.R., 2007. Stable hydrogen and oxygen isotope composition of waters from mine tailings in different climatic environments. Environ. Sci. Technol. 41 (6), 1870–1876.
Spiro, B., Chong, G., 1996. Origin of Sulfate in the Salar de Atacama and the Cordillera de la Sal, Initial Results of an Isotopic Study. *Third ISAG, St.* Malo (France) 17-19/9/1996, pp. 703–705.
Squyres, S.W., Knoll, A.H., 2005. Sedimentary rocks at Meridiani Planum: Origin, diagenesis, and implications for life on Mars. Earth Planet. Sci. Lett. 240, 1–10.
Stoertz, G.E., Ericksen, G.E., 1974. Geology of salars in northern Chile. Geol. Surv. Prof. Pap. 811, 1–67.
Taberner, C., Cendón, J.J., Pueyo, J.J., Ayora, C., 2000. The use of environmental markers to distinguish marine vs. continental deposition and to quantify the significance significance of recycling in evaporite basins. Sediment. Geol. 137 (4), 213–240.
Tapia, P.M., Fritz, S.C., Baker, P.A., Seltzer, G.O., Dunbar, R.B., 2003. A late Quaternary diatom record of tropical climatic history from Lake Titicaca (Peru and Bolivia). Palaeogeogr. Palaeoclimatol. Palaeoecol. 194, 139–164.
Taylor, B.E., Wheeler, M.C., Nordstrom, D.K., 1984. Isotope composition of sulphate in acid mine drainage as measure of bacterial oxidation. Nature 308 (5), 538–541.
Thode, H.G., Monster, J., 1965. Sulfur-isotope geochemistry of petroleum, evaporites and ancient seas. Am. Assoc. Petroleum Geologists Mem. 4, 367–377.
Thollot, P., Mangold, N., Ansan, V., Le Mouelic, S., Milliken, R.E., Bishop, J.L., Weitz, C. M., Roach, L.H., Mustard, J.F., Murchie, S.L., 2012. Most Mars minerals in a nutshell: Various alteration phases formed in a single environment in Noctis Labyrinthus. J. Geophys. Res. Planets 117.
Thompson, L.G., Davis, M.E., Mosley-Thompson, E., Sowers, T.A., Henderson, K.A., Zagorodnov, V.S., Lin, P.N., Mikhalenko, V.N., Campen, R.K., Bolzan, J.F., Cole-Dai, J., Francou, B., 1998. A 25,000-year tropical climate history from Bolivian ice cores. Science 282, 1858–1864.
Toran, L., Harris, R.F., 1989. Interpretation of sulfur and oxygen isotopes in biological and abiological sulfide oxidation. Geochim. Cosmochim. Acta 53 (9), 2341–2348.
Tosca, N.J., McLennan, S.M., 2006. Chemical divides and evaporite assemblages on Mars. Earth Planet. Sci. Lett. 241, 21–31.
Tyson, G.W., Chapman, J., Hugenholtz, P., Allen, E.E., Ram, R.J., Richardson, P.M., Solovyev, V.V., Rubin, E.M., Rokhsar, D.S., Banfield, J.F., 2004. Community structure and metabolism through reconstruction of microbial genomes from the environment. Nature 428 (6978), 37–43.
Utrilla, R., Pierre, C., Ortí, F., Pueyo, J.J., 1992. Oxygen and Sulphur isotope compositions as indicators of the origin of Mesozoic and Cenozoic evaporites from Spain. Chem. Geol. 102, 229–244.
Varekamp, J.C., Ouimette, A.P., Herman, S.W., Flynn, K.S., Bermudez, A., Delpino, D., 2009. Naturally acid waters from Copahue volcano, Argentina. Appl. Geochem. 24, 208–220.
Vita-Finzi, C., 1959. A Pluvial Age in the Puna de Atacama. Geogr. J. 125 (3/4), 401–403.
West, M.D., Clarke, J.D.A., Thomas, M., Pain, C.F., Walter, M.R., 2010. The geology of Australian Mars analogue sites. Planet. Space Sci. 58 (4), 447–458.
Wörner, G., Schildgen, T.F., Reich, M., 2018. The Central Andes: elements of an extreme land. Elements 14, 225–230.
Zaikova, E., Benison, K.C., Mormile, M.R., Johnson, S.S., 2018. Microbial communities and their predicted metabolic functions in a desiccating acid salt lake. Extremophiles 22 (3), 367–379.
Zodrow, E.L., Wiltshire, J., McCandlish, K., 1979. Hydrated sulfates in the Sydney coalfield of Cape Breton, Nova Scotia. II. Pyrite and its alteration products. Can. Mineral. 17, 63–70.